Annu. Rev. Nucl. Part. Sci. 1997. 47:663–709

COLLECTIVE FLOW IN HEAVY-ION COLLISIONS

W. Reisdorf
Gesellschaft für Schwerionenforschung, D-64220 Darmstadt, Germany

H. G. Ritter
Nuclear Science Division, Lawrence Berkeley National Laboratory, Berkeley, California 94720; e-mail: hgritter@lbl.gov

ABSTRACT

We provide an overview of collective flow phenomena observed in heavy ion collisions from the Fermi energy range up to CERN Super Proton Synchrotron (SPS) energies. We summarize the experimental data in terms of the various observed aspects of flow, namely directed flow in the reaction plane, elliptic flow in- and out-of-plane, and azimuthally symmetric radial flow originating from the expansion of the hot and compressed reaction zone. Also reviewed are the theoretical concepts developed to simulate the complex reactions with the aim of extracting fundamental properties of hot and compressed nuclear matter.

CONTENTS

1. INTRODUCTION 664
2. THE REACTION PLANE 665
3. IN-PLANE FLOW 667
   3.1 Flow of Nucleons and Clusters 667
   3.2 Flow of Produced Particles 676
   3.3 Disappearance of Flow 678
4. OUT-OF-PLANE FLOW 681
   4.1 Flow of Nucleons 681
   4.2 Flow of Produced Particles 685
5. RADIAL FLOW 687
   5.1 The Data 687
   5.2 Theoretical Considerations 694
6. AGS AND CERN ENERGIES 698
   6.1 Directed Flow 698
   6.2 Radial Flow 701
7. SUMMARY AND OUTLOOK 704

0163-8998/97/1201-0663$08.00

1. INTRODUCTION

Two heavy nuclei can be compressed to more than ground-state saturation density and heated in head-on collisions at high energy. A flow pattern will develop as the system subsequently expands. In macroscopic classical physics flow can be described in the language and with the tools of hydrodynamics (1–3), where one links in a conceptually simple way conservation laws (mass, momentum, energy) with fundamental properties of the fluid: the equation of state and transport coefficients, such as viscosity and heat conductivity.

The equation of state (EoS) of nuclear matter, i.e. the relationship specifying how the pressure, or alternatively the energy per particle, depends on density and temperature, is of fundamental interest. It is relevant to astrophysical events and objects such as the big bang, supernovae explosions, and neutron stars. It is generally accepted that nuclear matter should undergo at least two phase transitions: the liquid-to-vapor transition at temperatures below 20 MeV and at low density, and the deconfinement phase transition from hadronic matter to the quark-gluon plasma at high temperatures (larger than 150 to 200 MeV) and high energy density (5 to 10 times the ground-state density). One of the properties characterizing the EoS is the incompressibility K, which measures the resistance against compression (stiffness) and is expected to directly influence flow phenomena.

In 1955 Belenkij and Landau (4) first used a fluid-dynamics model to describe collisions of nucleons and nuclei. In 1959 Glassgold, Heckrotte, and Watson (5) considered the shock waves that could be formed when a high-energy proton or pion exceeding the nuclear speed of sound passes through a nucleus. They proposed a way to determine the nuclear compressibility coefficient. In the mid-1970s a number of theoretical papers assumed that hydrodynamics was governed by the formation of a shock wave (6–11) that most of the studies found propagating in the longitudinal direction.

The importance of *transverse* expansion was first shown by Scheid, Müller, and Greiner (7) in an ideal-fluid hydrodynamics calculation. For beam energies as low as 12.5A MeV, it was predicted that in the first 15 fm/c after penetration the transverse border of the stopped and shocked matter was expanding faster than the longitudinal border. The authors concluded matter is pushed outwards perpendicular to the relative motion of the two nuclei (7).

Experimentally, the first convincing evidence for the occurrence of sideward flow (12, 13) was obtained by so-called 4π detectors, the Streamer Chamber (14) and the Plastic-Ball/Wall (15) at the Bevalac in Berkeley. These detectors could fully characterize events by identifying and measuring the momenta of most of the emitted charged particles. The data (12) could be reproduced in a theoretical analysis (16) confirming a long series of predictions based on fluid dynamics (2).

Meanwhile, the field has grown and spans an energy regime of nearly five orders of magnitude (about 30*A* MeV to 200*A* GeV). A large amount of data has been accumulated. In this review of flow phenomena we follow a historic path. The occurrence of sideward flow requires the existence of a reaction plane that must be accessible to experimental observation (Section 2). So-called directed flow can be studied within the reaction plane (Section 3) or out of the reaction plane (Section 4). Besides directed flow there exists an azimuthally symmetric flow component that we shall term radial flow (Section 5). We have chosen to treat the high-energy data obtained at BNL/AGS and CERN/SPS separately (Section 6) and, for reasons of space limitations, rather briefly; related reviews covering the highest energies have been published very recently in this series (17–19). The interested reader will also find complementary information in the most recent Quark Matter proceedings (20).

In general, after presenting some of the available data, we discuss recent theoretical developments insofar as they are directly connected with flow phenomena. We look at efforts to extract information on the complex dynamics from these models with the goal of drawing conclusions about the properties of compressed and/or heated nuclear matter. The validity of hydrodynamics in the nuclear context was (and still is) a controversial issue (21). The mid-1980s witnessed the advent of sophisticated microscopic transport theoretical approaches specifically designed to overcome one of the possible shortcomings of fluid dynamics, the assumption of local equilibration. This assumption should be unrealistic both in the early (approach) phase of the collision, and in the final "freeze-out" phase when the nuclear system has expanded well below ground-state density.

2. THE REACTION PLANE

Observation of directed flow requires that a reference plane—the reaction plane—exists. We shall use the Cartesian coordinates x, y, z with the convention that the unit vector $\hat{z}$ points in the beam direction, while $\hat{x}$ is in the reaction plane. Historically, the reaction plane was first determined with the sphericity method (12, 22, 23). For each event the 3×3 kinetic-flow tensor is defined separately:

$$F_{ij} = \sum_{\nu} p_i(\nu) p_j(\nu)/m_\nu \quad i, j = x, y, z \qquad 1.$$

with $p_i(\nu)$ being the components of the momentum vector of the individual particle ν and m_ν being its mass. The sum runs over all particles in the entire event. The tensor is symmetric by construction and hence is defined by six independent numbers. Diagonalization allows the determination of three variables, usually the three eigenvalues $\lambda_3 > \lambda_2 > \lambda_1$ (which geometrically represent the

shape of an ellipsoid) and three other angular variables (giving the orientation of the ellipsoid in space). One of the shape variables is an overall scaling quantity given by energy conservation (and hence should permit a consistency check in 4π experiments). The angle between the eigenvector $\hat{e}_3$ associated with the largest eigenvalue λ_3 and the beam axis z is called the flow angle, θ_f. The reaction plane is spanned by $\hat{e}_3$, the flow axis, and the beam axis. Sometimes it is useful to rotate the coordinate system around the y-axis by the flow angle, θ_f. The new coordinate system agrees with the major axis of the flow ellipsoid and is denoted by x', y', z' with z' being the flow axis and $y' = y$ (see Figure 3 in Reference 24).

Danielewicz and Odyniec (25) have introduced the transverse momentum method to determine the reaction plane spanned by the vector

$$\vec{Q} = \sum_{\nu} w_\nu \vec{p}_t(\nu) \qquad 2.$$

and the z (beam) direction. The weight w_ν is usually chosen to be $+1$ at forward center-of-mass rapidities and -1 at backward rapidities, so that $\vec{Q}$ is a measure for the collective transverse-momentum transfer between the forward and backward hemispheres. Finite-number and other sources of fluctuations, as well as experimental cuts and distortions, lead to an uncertainty in the orientation of $\vec{Q}$. This uncertainty is often estimated with the subevent method (25). The quality of the reaction-plane determination depends on the number of particles in the event and on the strength of the flow effects. Some flow observables can also be obtained with methods that do not require *explicit* determination of the reaction plane and hence avoid the need to correct for finite-number deviations from the true reaction plane (26).

An alternate way to determine the reaction plane is to perform a high-precision measurement of the transverse momentum of the heaviest fragment produced in intermediate-impact-parameter reactions.

Directed-flow effects can also be characterized by the azimuthal distribution of the emitted particles, $dN/d\Phi$,

$$dN/d\Phi = c(1 + a_1 \cos(\Phi) + a_2 \cos(2\Phi)), \qquad 3.$$

where Φ is the azimuthal angle relative to the reaction plane. This simple description takes only number effects into account and does not include the momenta of the measured particles. The coefficient a_1 represents the strength of the first moment, directed flow in the reaction plane with preferred emission at 0° in the forward hemisphere and 180° in the backward hemisphere. a_2 measures the strength of the second moment, i.e. it represents a flattening of the ellipsoid. A positive value results from preferred out-of-plane emission with maximal emission at 90° and 270° relative to the reaction plane (see

Section 4). There is no experimental evidence yet that higher terms need to be taken into account. If particle emission is studied in the coordinate system of the flow ellipsoid, the first moment is minimized and the second moment is maximized.

There is interest in using observables that are both coalescence- (27) and scale-invariant. Coalescence-invariant observables allow comparison with theories that are limited to making predictions for single-particle observables. Under certain conditions (28) the evolution in nonviscous hydrodynamics does not depend on the size of the system nor on the incident energy, if distances (such as impact parameters) are rescaled (reduced) in terms of a typical size parameter, such as the nuclear radius. Velocities, momenta and energies are rescaled in terms of the beam velocities, momenta or energies. Although the scaling conditions appear to be very restrictive, it is still useful to consider flow observables that are scale-invariant and thereby try to remove trivial consequences from size and incident velocity variations.

3. IN-PLANE FLOW

3.1 *Flow of Nucleons and Clusters*

3.1.1 THE DATA Since the unambiguous discovery of sideward flow (12, 13), a large number of experimental studies have been done (25, 26, 29–56). Most of the data on directed flow were analyzed with the transverse momentum method (25). The average transverse momentum per nucleon in the reaction plane $\langle p_x/A\rangle(y)$ is plotted as a function of rapidity y. Figure 1 shows the S-shaped curve characteristic of the collective transverse-momentum transfer. The sign changes at the point y_c, which for symmetric systems is identical to the center-of-mass (c.m.) rapidity. By convention p_x is defined to be positive in the forward hemisphere if repulsive effects are dominant, i.e. if projectile and target nucleons are predominantly diverted away from each other. The data are from the EOS Collaboration (52) for protons and alpha particles produced in Au+Au collisions at 800A MeV. It is obvious that flow effects are larger for the heavier fragments (36).

The Plastic Ball Collaboration (31) characterized sideflow by the slope of the curve $F = d\langle p_x/A\rangle/dy_n$ taken near the zero cross-point y_c, where y_n is the normalized rapidity, defined to be $+1$ (-1) at projectile (target) rapidity. The choice of normalized rapidity has the advantage that the rapidity distributions of the nucleons seem to scale. If one wants to use a scale-invariant observable for the flow as well, it is better to use the quantity $F_y = d\langle p_x/A\rangle/dy$ with the unmodified rapidity y. Close to y_c the observable F_y is within a constant (the nucleon mass) equivalent to $F_u = d\langle u_x\rangle/du_z$, where $u_{x,z}$ are four-velocity components in the c.m. system.

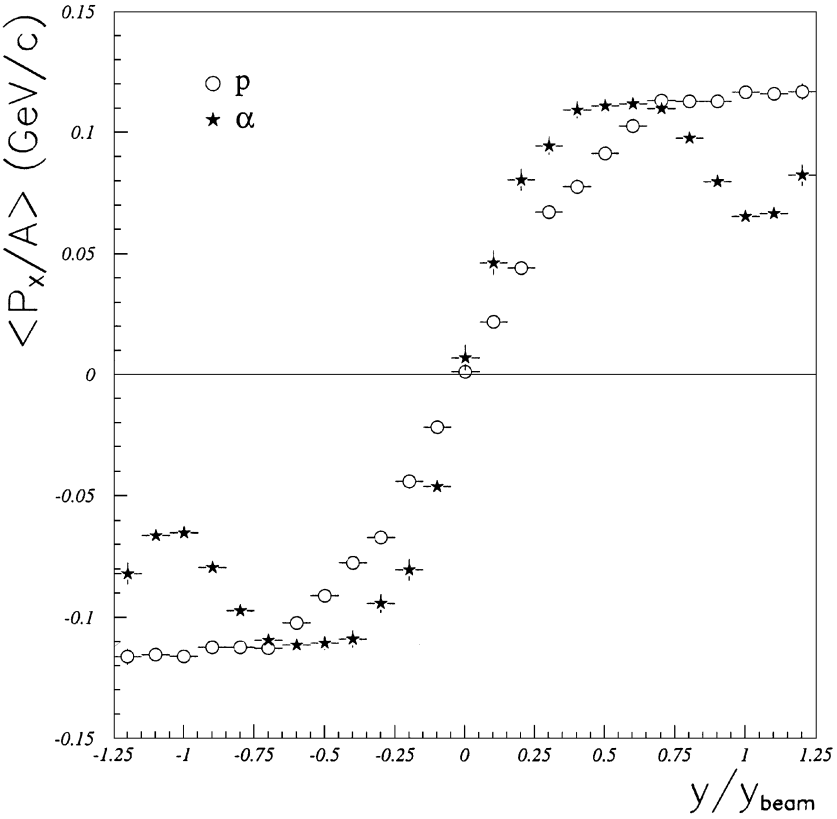

Figure 1 Average in-plane transverse momentum versus normalized rapidity in the reaction Au+Au at 800*A* MeV. The points at $y/y_{beam} < 0$ are reflected.

There are alternative (coalescence-invariant) ways to quantify sideflow. The directivity, D, is a measure for the alignment of particles (34, 57):

$$D = \left| \sum_i A_i \vec{u}_{ti} \right| \Big/ \sum_i A_i |\vec{u}_{ti}|. \qquad 4.$$

Here the scaled four-velocity $u \equiv (\vec{u}, u_4)$ has been introduced: $\vec{u} = \vec{\beta}\gamma/\beta_p\gamma_p$, where $\vec{\beta}$ is the velocity in units of c, $\gamma = (1-\beta^2)^{-1/2}$; $u_4 = \gamma/\gamma^p$ and the index p refers to the incident projectile in the center-of-mass system. Another very useful quantity is F_{DO} (25, 58):

$$F_{\mathrm{DO}} = \sum_{j,i\neq j} A_i \vec{u}_{ti} A_j \vec{u}_{tj} \Big/ \sum_{j,i\neq j} A_i A_j. \qquad 5.$$

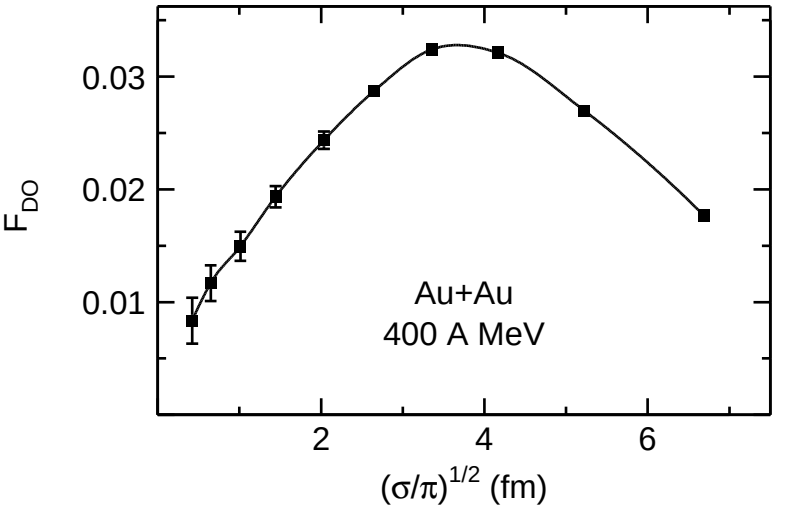

Figure 2 Centrality dependence of the flow variable, F_{DO}.

In experiments where the nuclear charges, Z_i, but not the masses, A_i, are resolved, A_i is usually replaced by Z_i. Although these global observables are not all identical, they tend to lead to qualitatively similar trends as a function of impact parameter, system size, and energy.

Sideflow data are usually presented for intermediate impact parameters, where the values are largest (31). The most common way of selecting the impact parameter is by binning the total observed charged particle multiplicity (59). For zero impact parameter, sideflow must be zero by symmetry. For very peripheral collisions it is expected to converge to zero as well. In Figure 2 a typical impact-parameter dependence is shown (48, 60). Here an alternative selection, varying the global ratio of transverse to longitudinal kinetic energies (60), has been used, converting cross sections to impact parameters with a sharp-cut geometrical model. Over a large range of beam energies (48) the peak is near the scaled impact parameter $\hat{b} = b/b_{max} = 0.25 - 0.30$ (3.5–4 fm for Au+Au).

Figure 3 shows the Z-dependence of sideflow (56) by plotting the equivalent angle, $\theta_s = \arctan(F_u)$, as a function of the charge of the fragment. One notices a tendency towards saturation as $Z > 3$ (61). If flow is characterized by a constant velocity field superimposed on the random thermal motion, the ratio between flow velocity and random motion becomes very large as the particles become heavier. Thus the heavy-mass fragment value of θ_s converges toward the flow angle, θ_f (56).

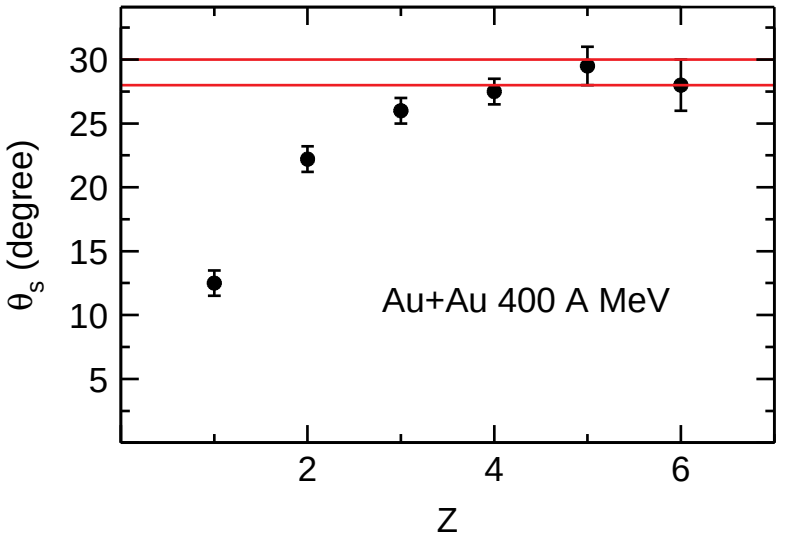

Figure 3 Apparent flow angles in Au+Au (400*A* MeV) as a function of the fragment charge.

Figure 4 gives an overview of flow data for symmetric systems of varying size as a function of beam energy. Data from the Plastic Ball (62), the EOS (52, 55), and the FOPI (56) Collaborations are used. Flow values are taken from intermediate-impact-parameter bins where the values reach a maximum. With the exception of the FOPI data, which represent the asymptotic values illustrated in Figure 3, sideflow was determined from particles with charge one and two. F_y increases as a function of energy up to about 250*A* MeV. Beyond 400*A* MeV it decreases again. If calculated with normalized rapidity, the flow continues to increase (31). Sideflow tends to be smaller for lighter systems, in contradiction to ideal-fluid dynamics, which predicts constant flow. Flow of heavier fragments is larger (36); the FOPI values for Au+Au with intermediate-mass fragments (IMF) are larger by about a factor 1.4 compared to the values calculated using light fragments (52, 62). Wang et al (53) have applied a simple coalescence prescription (27) to their data and found that the increase in slope can be reproduced for the light fragments if a transverse momentum cut of 250 MeV/*c* is used.

An empirical scaling rule introduced by the EOS Collaboration (55) allows to compare flow values for symmetric and asymmetric systems of different size. When the flow value F_y is scaled for the system size, $F_S = F_y/(A_1^{1/3} + A_2^{1/3})$, the scaled values plotted as a function of energy all fall in a relatively narrow band.

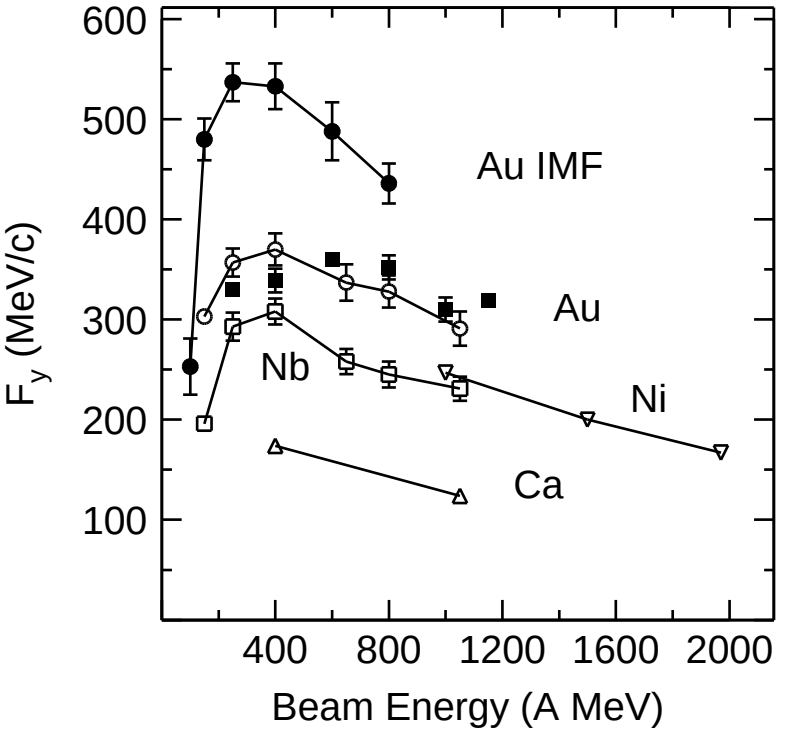

Figure 4 Sideflow, F_y, in symmetric systems.

The study of asymmetric systems offers new, more complex information. The basic geometry, and hence the initial conditions, is different from the symmetric case. Strictly speaking, one system cannot be reduced to the other by simple rescaling, even in the ideal-fluid situation.

In asymmetric systems one expects $\langle p_x(y)\rangle$ to cross zero at a value $y = y_c$ that is intermediate between the center-of-mass of the full (compound) system and that of the nucleon-nucleon system. A precise measurement of the crossing point should allow determination of the size of the fireball system and of the effective number of participants. It also should shed light on the mechanism of stopping. If cross talk between the overlap region and the spectators is large, the fireball will be larger and the zero-crossing point will be closer to the compound c.m. Conflicting results are presented in the literature. Beavis et al (44) found that the number of participants deduced from the zero-crossing point strongly increased as the incident energy was lowered from 1800*A* to 400*A* MeV for

the reaction Ar+Pb. In contrast, in the reaction Ni+Au (55) the zero-crossing point was at almost constant normalized rapidity over a comparable energy range.

One does not expect the function $\langle p_x/A\rangle(y)$ (the S-shaped curve) to be symmetric relative to the crossing point in asymmetric systems. There is the obvious constraint that the rapidity-integrated total momentum transfers on both sides must cancel. The side with fewer participants will have a larger transverse momentum *on a per-nucleon basis*. This explains the relatively large sideward flow (even after using the size-scaling prescription of Reference 55) found in the forward (light-projectile) hemisphere (26, 55).

3.1.2 THEORETICAL ANALYSES The search for flow was stimulated by hydrodynamic considerations. During the course of the collision, nuclear matter is compressed and the pressure field buildup leads to flow in the expansion stage (2). This flow must have a directional component since noncentral collisions always have a defined reaction plane. Originally it was hoped that the amount of transverse flow could be directly related to the stiffness of the equation of state (22).

The dependence of the flow angle, θ_f, on the impact parameter, b, the incident energy, the EoS, and viscosity was studied in the framework of one-fluid viscous hydrodynamics (63). For a fixed energy, the hydrodynamic flow angle seems to be primarily governed by geometry: for $b = b_{max}$ it is zero and increases smoothly to 90° for $b = 0$. The biggest variation between different EoS and viscosities is just 7° around $b/b_{max} = 0.2$. Fixing b/b_{max} to be 0.2, θ_f is almost independent on energy (200 to 800A MeV); again, typical variations with the EoS or viscosity are just about 5°. The only significant modification of sideflow in this model concerns the in-plane transverse momenta near target or projectile rapidity that are found to be influenced by viscosity. It is intuitively clear that shear viscosity will inhibit cross talk between the almost stopped fireball and the almost undecelerated spectator parts. Thus, according to this model, it is not the mid-rapidity slope, F_y, that is instructive, but rather the transverse momenta in the spectator regions! This has not yet been addressed in the experiments.

In the experiment two things are different: (*a*) Flow is measured with a finite thermal resolution that depends on the particle mass. Thermal motion affects protons much more strongly than the alphas that stay close to the hydro-flow (63, 64). This explains the experimental observation that the mid-rapidity slope, F_y, is larger for heavier particles (see Figure 1). However, for light particles the effect can also be explained within a coalescence picture (53, 65). (*b*) The experiment cannot detect the 90° flow, predicted at $b = 0$, with the usual transverse momentum or sphericity method because the reaction plane accuracy dramatically decreases as $b \to 0$.

As noted earlier, in ideal-fluid hydrodynamics, properly scaled flow observables are not expected to depend on the size of the system, nor on the incident energy. It can be seen in Figure 4 that this is in contradiction to the data. Deviations from scaling can be due to many reasons: nonideal EoS behavior, such as saturation of the temperature at very high incident energies (6), a phase transition (66), or a change in the freeze-out conditions, possibly due to a modification of the chemical composition of the fluid. Changes in viscosity can also cause modifications in flow patterns. An apparent correlation of flow data with Reynolds number was demonstrated for energies above 150*A* MeV (66, 67). The Reynolds number is inversely proportional to the viscosity and has a length scale implying an $A^{1/3}$ dependence, as suggested by Chance et al (55). In elementary kinetics, the viscosity would be inversely proportional to the nucleon-nucleon scattering cross section, σ_{nn}.

Another consequence of finite viscosity is that shock profiles have a finite width. Using realistic viscosities derived from Uehling-Uhlenbeck equations, Danielewicz (68) estimated that the widths of shock profiles were about 4.5 fm at 100*A* MeV and 1.8 fm at 800*A* MeV. He concluded that shock phenomena are not possible below about 100*A* MeV, while at higher energies a fully developed shock would require systems with mass $A \geq 100$. Qualitatively, the decrease of flow below 150*A* MeV and the small flow in the Ca+Ca system support this conclusion.

A theoretical framework that avoids some of the assumptions necessary to justify the use of fluid dynamics is that of semiclassical transport theories such as cascade codes (69–72) and Boltzmann-Uehling-Uhlenbeck codes (BUU) (73–75) or Quantum Molecular Dynamics (QMD) (76). Those codes microscopically describe the evolution from a non-equilibrium configuration into one that is possibly, but not necessarily, thermal.

Cascade codes simulate the nuclear interaction by a succession of stochastic scatterings between individual particles with measured cross sections (where known). They do not include mean-field effects and thus implicitly assume an EoS that should be close to that of an ideal gas. Even though these codes show some residual effects, they cannot reproduce the measured flow values (77). More recently, the intranuclear cascade code ARC (72) reports agreement with EOS sideward flow data (78). The codes that produce apparently different results differ in some assumptions they make about the scattering style, i.e. the treatment of angular momentum (plane) conservation in two-body collisions and the choice of repulsive versus attractive orbits. While it is important that such differences among various codes are resolved, it is much more important for the understanding of nuclear collisions to find out what form the "effective" equation of state generated by different assumptions might have (79).

In transport codes such as BUU (73, 74) or QMD (76), propagation between collisions is controlled by the mean field. The mean field or single-particle

potential $U(\rho, p)$, is a functional derivative of the interaction energy for the system, and is directly related to the nuclear matter equation of state. The single-particle potential has frequently been assumed to take some relatively simple form, such as the Skyrme parameterization:

$$U(\rho) = a(\rho/\rho_o) + b(\rho/\rho_o)^\sigma. \qquad 6.$$

Usually, the parameters a, b, and σ are constrained to fit given properties of saturating nuclear matter: binding energy per nucleon, saturation density, incompressibility K. In the nuclear physics context $K = R^2 d^2(e/\rho)/d^2 R$, where the second derivative is taken for constant mass number and entropy and e is the energy density (the underlying picture is that of the stiffness against a change of the nuclear radius R relevant in studies of nuclear breathing modes). For the incompressibility, two options, $K = 200$ MeV ("soft," or S) and $K = 380$ MeV ("hard," or H), are frequently used. Attempts to explain pion-production data (80, 81) and collective flow (12) with this form of $U(\rho)$ led to the conclusion that the equation of state must be very stiff (82, 83) in disagreement with microscopic calculations based on Hamiltonians fit to nucleon-nucleon scattering data (84), and attempts to deduce the equation of state from supernova simulations (85).

The parametrization of Equation 6 neglects the momentum dependence of the real part of the optical nucleon-nucleus potential which is known to become repulsive around 300 MeV and converges toward 30 MeV for very high nucleon momenta. The effect of the momentum dependence of $U(\rho, p)$ was first studied by Gale, Bertsch, and DasGupta (86) and by Aichelin (87) using phenomenological Ansätze and was further developed by Welke et al (88) and Haddad et al (89). It was found that an equation of state with an incompressibility of about 215 MeV and a reasonable $U(\rho, p)$ could fit then-available data as well as a stiff equation of state without momentum dependence.

However, mean-field Ansätze $U(\rho, p)$ that reproduce equilibrium properties of nuclear matter and finite nuclei may well differ in the extreme non-equilibrium situation that prevails in the earliest phase of heavy-ion collisions. This might influence later stages, e.g. the maximal density that is reached. Intuitively, one expects that the momentum dependence is best determined in reactions with small compression, e.g. in light symmetric systems or in very asymmetric systems, or in more peripheral collisions. With the momentum dependence fixed, the study of central collisions of heavy symmetric systems, where higher compressions are achieved, might fix the incompressibility (75, 90).

With BUU simulations, Pan and Danielewicz (91), using sideward flow data (F) from both Plastic Ball [for Nb+Nb (38)] and Diogène [for Ar+Pb (41)] showed that the hard (H) versus soft-momentum-dependent (SM) ambiguity could be resolved. They excluded H, primarily because the high-p_t data in

the Diogène experiment required explicit momentum dependence (but were relatively insensitive to the incompressibility). They also claimed that measured rapidity distributions required that the in-medium nucleon-nucleon cross sections, σ_{NN}, be larger than 65% of the free scattering cross sections, thus limiting the freedom to manipulate the flow predictions by varying σ_{NN}. They concluded that the soft and momentum-dependent version with a nuclear matter incompressibility, K, in the range of 165–220 MeV best described the data.

The results of Pan and Danielewicz (91) were corroborated by independent BUU calculations (89, 92). Very recent sideflow data (61, 93), extending to large impact parameters, also confirm the necessity for momentum-dependent mean fields.

A better understanding of the momentum dependence of the potentials requires relativistic theories. Relativistic Transport theories (RBUU) (74, 94) have been developed within the framework of Walecka's (95) nonlinear σ–ω model. Here the nucleon-nucleon interaction is described by the exchange of an attractive scalar meson and a repulsive vector meson. The original version of the model allows only for a linear energy dependence of the mean field potential and thus cannot reproduce the experimental nucleon-nucleus optical potential over a large energy range. Therefore, an extension of the σ–ω model was necessary to achieve consistency with experiments (96).

In the context of sideflow, some of the results (96, 75) obtained with RBUU are as follows: The $\langle p_x(y)\rangle$ observable seems rather insensitive to any mean-field variation. This is reminiscent of the conclusions reached from fluid dynamics, discussed above. There is a somewhat higher sensitivity to the directivity distribution (Equation 4). The generation of the transverse momenta has three sources of comparable importance: the mean-field potential, which (at 800A MeV, for example) in a relatively narrow transition zone between compressed and spectator matter (the shock-profile zone in the language of hydrodynamics) is repulsive, the "cross talk" between spectators and participants due to collisions in the participant matter (kinetic pressure in hydrodynamics), and the Fermi motion from spectator nucleons into participant matter.

Although the momentum-dependent potentials (87, 88, 96) all fulfill the condition that they reproduce the energy dependence of the real part of the optical nucleon-nucleus potential, determined at normal nuclear density, it is not clear that the extension to other densities contains the correct physics. It is therefore desirable to try to derive the function $U(\rho, p)$, as well as the effective in-medium cross sections, from a more microscopic approach such as deriving the G matrix from a realistic nucleon-nucleon potential by self-consistently solving the Bethe-Goldstone (nonrelativistic) or the Bethe-Salpeter (relativistic) equation. These theories, applied to relatively light systems such as Ca+Ca at 400A MeV (97) and Ar+KCl at 1.8A GeV (98), showed that the mean fields derived from a G-matrix calculation (both relativistic and nonrelativistic) were more repulsive

(and hence generated more sideward flow) than comparable phenomenological mean fields. A study (99) where the mean field was approximately calculated from local *two*-Fermi sphere configurations reproduced Au+Au data well at 400*A* MeV (51).

Since the collisional part of these increasingly complex transport calculations is as important as the mean-field part for many of the observables, in particular the sideward flow, it seems necessary to extend the microscopic calculations also to the cross sections, i.e. the imaginary part of the *G*-matrix. Finally, sideward flow is sensitively dependent on surface effects, which are often influenced by more technical parameters (100–102) in the transport calculations. These need to be treated realistically, especially for light systems, such as C+C (101).

3.2 *Flow of Produced Particles*

3.2.1 PIONS Due to their small mass, pions are not expected to show considerable flow effects if flow is represented by a common velocity superimposed on the thermal motion. On the other hand, pions are subject to absorption and re-emission. The heavy deltas should show flow behavior very similar to that of the protons (103, 104).

The correlation between nuclear flow and pion emission was first measured and analyzed by the Diogène Collaboration (105). In Ne collisions with NaF, Nb, and Pb at 800*A* MeV the reaction plane has been determined from identified protons using the transverse-momentum method. $\langle p_x \rangle / A$ has been determined as a function of rapidity for charged pions. The astonishing result was that charged pions show positive $\langle p_x \rangle$ values for all rapidities, indicating that they are preferentially emitted towards the light projectile side, away from the heavy target. This behavior was interpreted as an absorption of pions in the target remnant, leading to a preferred emission towards the other side.

In-plane average transverse momenta of pions have been measured for Au+Au at 1*A* GeV (106) and 1.15*A* GeV (107). Qualitatively similar observations were made in both experiments. For sufficiently high impact parameters ($b > 5$ fm) a weak "antiflow" signal was observed for positively charged pions, i.e. the sign of $\langle p_x \rangle$ was opposite that of protons in the same rapidity interval. For π^- the effect is weaker and limited to more peripheral reactions. If the apparent antiflow is just an absorption effect, central collisions with little or no spectator matter should show no flow or a small positive flow signal (103, 104). This has been observed in the data, but the effect is small and the statistics is marginal. This can be interpreted as a faint remnant of the parent Δ flow.

Microscopic transport models for the energy range around 1*A* GeV generally assume that pions are produced almost exclusively as decay products of the Δ resonance ($N + N \rightarrow \Delta$; $\Delta \rightarrow \pi + N$). After its formation the Δ as well as the π can undergo rescattering ($N + \Delta \rightarrow N + \Delta$, $\pi + N \rightarrow \Delta \rightarrow \pi + N$) or the Δ can be absorbed again ($N + \Delta \rightarrow N + N$). In order to be realistic

such calculations must take into account isospin and Coulomb effects, detailed balance, and the correct finite resonance life time. Within the BUU model (108, 104) it was shown that in the Diogène reaction (Ne+Pb) virtually no pion "flow" was produced if both rescattering and absorption effects were shut off in the calculations, while the full calculation was able to reproduce the data (105). The EOS data (107) can also be reproduced by BUU calculations (107–109). Detailed calculations were also done using the VUU (110) and QMD (103) approaches. The authors selectively deactivated the rescattering ($\pi + N \rightarrow \Delta \rightarrow \pi + N$) and the "true absorption" ($N + \Delta \rightarrow N + N$) processes and concluded that "antiflow" was primarily produced by rescattering.

3.2.2 STRANGE PARTICLES Because of the relatively weak interaction of kaons with nucleons (10 mb), the measurement of kaons from heavy-ion collisions is considered to be a promising probe of the dense matter formed in the initial stage of the collisions. Recent theoretical work (111–113) has suggested that in-plane flow and azimuthal distributions of strange particles may provide useful information on in-medium properties of these particles.

Figure 5 shows very recent measurements (104) of Λ and K^+ flow and compares them to proton flow. Both the EOS Collaboration (115) and the FOPI Collaboration find that the Λ flow follows the nucleons. In contrast, the K^+, which are predominantly produced in association with the Λ, show very little flow. Furthermore, little flow was seen for K_s^0 and K^- mesons in the same reaction (114), although with less statistical significance. Due to the theoretical possibility of K^- condensation in dense stellar matter (116), experimental information for the K^- is particularly interesting, but difficult to obtain at energies below 2A GeV because of the low production cross sections.

Relativistic transport calculations (RBUU) applied to Ni+Ni at 1.9A GeV suggest the following picture for the Λ particles (113): the sideflow of the "primordial" Λ, which they acquire by the Lorentz boost of the parent baryons, represents only about half the final value. After production each Λ undergoes about 2.5 collisions with nucleons (the ΛN cross section is rapidly rising below 9.4 GeV/c), increasing the flow by another 20% of the asymptotic value. Finally, the rest of the flow originates from the attractive ΛN mean field (related in a simple constituent quark model to the nucleon mean field).

Systematic studies of in-medium properties of kaons have been carried out using chiral perturbation theory (117). It was shown that the K^+ in the nuclear medium feels both a strong vector repulsion and a slightly weaker scalar attraction. Calculations with RBUU (111) shown in the lower panel of Figure 5 suggest that sideward flow is sensitive to the assumed mean-field potential: in the absence of kaon propagation in a mean field (dashed line), the flow goes with the nucleons, but if the scalar part of the potential is suppressed (dashed line) a pronounced "antiflow" is seen. The experimental data seem to be reproduced

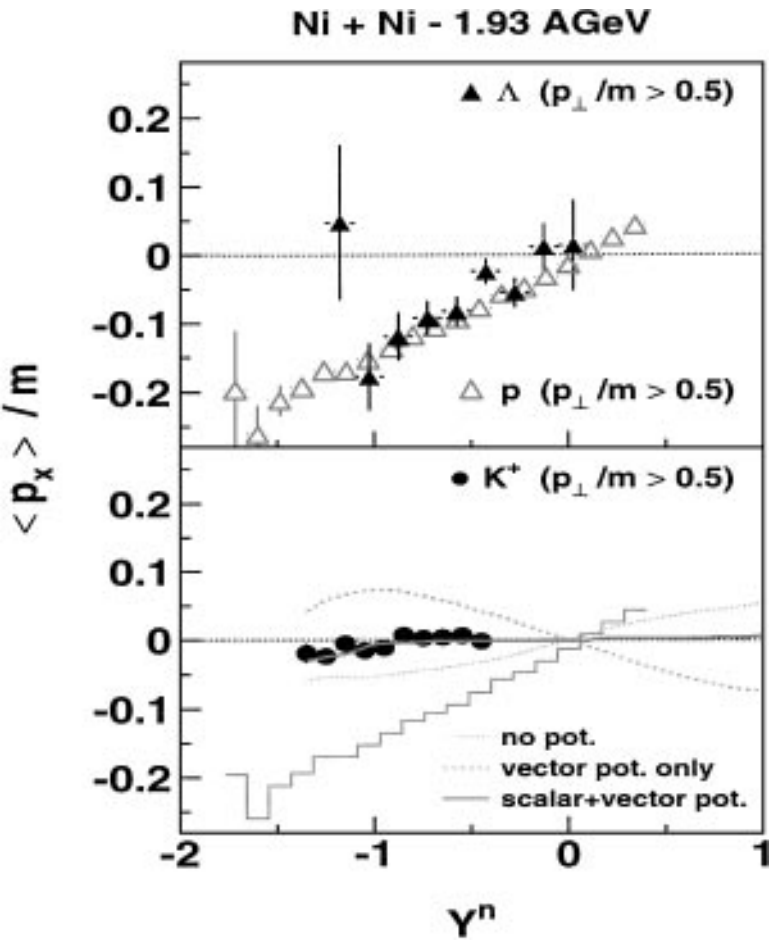

Figure 5 $\langle p_x \rangle / m$ as a function of scaled rapidity in the reaction Ni+Ni at 1.93*A* GeV. *Upper panel*: protons (open symbols) and lambdas (closed symbols). *Lower panel*: kaons (closed circles). The theoretical curves are from Reference 111.

when a more realistic potential is used. Experimental work, including the extension of the measurements to heavier systems, is needed. Further theoretical work is needed as well, as a consensus on the influence of rescattering on the spectra of strange particles has not yet been reached (118).

3.3 *Disappearance of Flow*

Directed flow disappears at an incident energy, termed the balance energy, E_{bal}, (119), where the mean field that is attractive at low energies is compensated

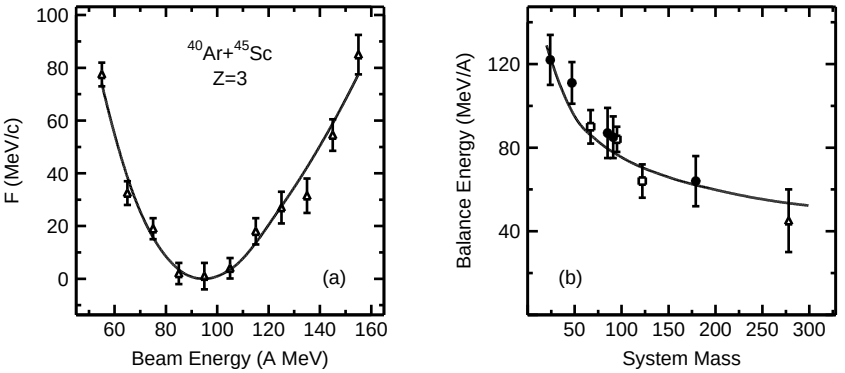

Figure 6 (*a*) Sideward flow, F, as a function of incident energy for ^{40}Ar+^{45}Sc, after Pak et al (93); (*b*) system-mass dependence of the balance energy. The lines suggest an $A^{-1/3}$ dependence.

by the repulsive action of nucleon-nucleon collisions. The disappearance of directed transverse flow is now well established by many experiments (93, 120–130).

Figure 6 shows a study (93) where the slope, F (not corrected for finite number effects), for Li fragments in the reaction ^{40}Ar+^{45}Sc at $\hat{b} = 0.39$ is followed over an energy range that is sufficient to establish both the decrease of the attractive flow and its re-emergence beyond 95A MeV rather well. On the low energy (attractive) side, the sign of the average emission angle of fast light particles (p, d, t, α) was determined (131) from the circular polarization of coincident γ rays (132) emitted from residual nuclei for ^{14}N-induced reactions on ^{154}Sm at $E/A = 20$ and 35 MeV. It was found that the particles were preferentially emitted to *negative* angles, consistent with the deflection of the particles by the attractive nuclear mean field.

Several studies (129, 130, 133) concur in observing that the balance energy seems to be weakly or not at all dependent on the emitted particle type under study. Furthermore, the balance energy was found to depend linearly on the impact parameter (129, 130). The system-size dependence for an average $b/b_{max} \approx 0.4$ is shown in panel (*b*) of Figure 6 (119, 120, 124, 128, 129, 133).

With Vlasov-Uehling-Uhlenbeck (VUU) calculations, Molitoris and Stöcker (83) had predicted a transition from the attractive regime at 50A MeV to the repulsive regime at 150A MeV for Nb+Nb ($\hat{b} = 0.24$). The question of a change of sign of $\langle p_x \rangle$ was also addressed by Bertsch and coworkers (134). Their BUU calculations with a Skyrme-type mean field and different (constant) nucleon-nucleon cross sections, σ_{NN}, predicted a balance energy between 60 and 100A MeV for reactions induced by $A_p = 40$ projectiles. They found that the predictions were influenced more strongly by the σ_{NN} values than by

the EoS and concluded that information on the latter could only be gained if the effective σ_{NN} were known rather well a priori. Also, the rise of E_{bal} with increasing impact parameter b was seen.

Since then many theoretical works concerned with the disappearance of flow have appeared (101, 119, 135–147). These calculations all confirm the findings just mentioned.

Around the balance energy, E_{bal}, the mean field, $U(\rho, p)$, is indeed still attractive and the compensation of its effect on the mid-rapidity slope, F_y, is due to the repulsive effect of hard nucleon scattering, i.e. σ_{NN} (147). As a general rule E_{bal} is lowered by an increase of repulsive effects either due to more centrality (more hard collisions) or by introducing momentum-dependent mean fields, which make the mean field more repulsive for high momenta and less repulsive for low momenta (146, 147). The effect of momentum dependence is subtle, however, as it leads to smaller densities, which in turn lower the repulsive effect of σ_{NN} (147). In principle the balance energy can be used to constrain in-medium effects in this energy range (50–150A MeV) where the effects of Pauli blocking are large. Overall, the use of in-medium (G-matrix) cross sections tends to lessen the repulsive effect of the hard collisions (147).

Reproduction of the experimental mass dependence (Figure 6) is not trivial. Following a simple argument (133) to understand the size dependence of E_{bal}, the attractive mean field should scale from proximity considerations with the surface of the two interacting nuclei, i.e. with $A^{2/3}$, while the repulsive hard collisions should scale with the overlapping volume, i.e. with A, resulting in the balance changing with $A^{-1/3}$. In VUU calculations using the nonlocal Gogny interaction (137), an $A^{-1/3}$ dependence of E_{bal} was extracted. In another calculation (101) without momentum dependence of $U(\rho, p)$, E_{bal} was underpredicted unless lower σ_{nn} (20%) were used, but then the predicted size dependence was too steep. A fair reproduction of the mass dependence could be achieved with use of nonrelativistic G-matrix mean fields and cross sections (147). Clearly further theoretical and experimental work is needed.

Coulomb effects are not negligible and could change the simple size scaling considerations made before. For very heavy systems, such as Au on Au, efforts to determine the balance energy (56, 123, 148) so far are inconclusive, since the balance energy has not been reached experimentally. Extrapolating from Wilczynski plots for low-energy deep-inelastic collisions, Gobbi et al (149) argue that sideflow is predominantly repulsive at *all* intermediate energies for very heavy systems. Soff et al (146) point out that the nuclear balance energy for Au+Au (which is predicted to be about 60A MeV for $b/b_{max} = 0.25$–0.5) can only be extracted after removal of the Coulomb rotation in the incoming and outgoing channels.

Li and Ko (150) predicted within the framework of a BUU calculation that the balance energy should be higher for more neutron-rich systems primarily

because the neutron-neutron cross section is about a factor of 3 smaller than the neutron-proton cross section in the relevant energy regime. A recent comparative experimental investigation (151) of sideflow in the systems ^{58}Ni+^{58}Ni and ^{58}Fe+^{58}Fe confirmed the isospin dependence of sideflow.

4. OUT-OF-PLANE FLOW

The coefficient a_2 in Equation 3 represents a deviation from a spherical shape of the ellipsoid and defines a second direction of preferred emission. The so-called squeeze-out has been identified first as such a phenomenon, leading to the term out-of-plane flow. From geometrical considerations, it is quite obvious that especially for reactions with intermediate impact parameters, emission out-of-plane is a much more direct and unobstructed way to radiate particles. Like sideflow, this is a collective effect and most of the models predicting collective effects, such as hydrodynamic or modern microscopic models that include some form of equation of state, predict this mechanism of particle emission (7, 10, 88, 152, 153).

Out-of-plane flow of nucleons is governed by different processes than the emission of produced particles (mainly pions). Therefore, the two phenomena are treated separately, with arguments closely following the discussions in Section 3.2.

4.1 *Flow of Nucleons*

Squeeze-out has been observed first by the Diogène Collaboration in Ne-induced reactions at 800*A* MeV (41). The Plastic Ball Collaboration has characterized the effect and performed a systematic analysis in Au+Au reactions (24, 154). Out-of-plane emission is strongest for reactions at intermediate impact parameters. The effect is most pronounced at mid-rapidity, but extends quite far towards projectile and target spectators, i.e. emission is not jet-like (152).

Squeeze-out is interesting as a collective phenomenon that preserves memory of the early high-density stage of the collision. The ratio R_N (24),

$$R_N = \frac{dN/d\Phi(90^\circ) + dN/d\Phi(-90^\circ)}{dN/d\Phi(0^\circ) + dN/d\Phi(180^\circ)} = \frac{1 - a_2}{1 + a_2}, \qquad 7.$$

measures the strength of the effect in a quantitative way. However, it only takes into account the azimuthal distribution and not the momenta of the emitted particles.

Figure 7 shows the energy and mass dependence of the squeeze-out ratio R_N measured by the Plastic Ball Collaboration (24). The energy dependence of R_N was compared with the energy dependence of sideflow (e.g. from Reference 31) and the question of why out-of-plane emission should have a different energy

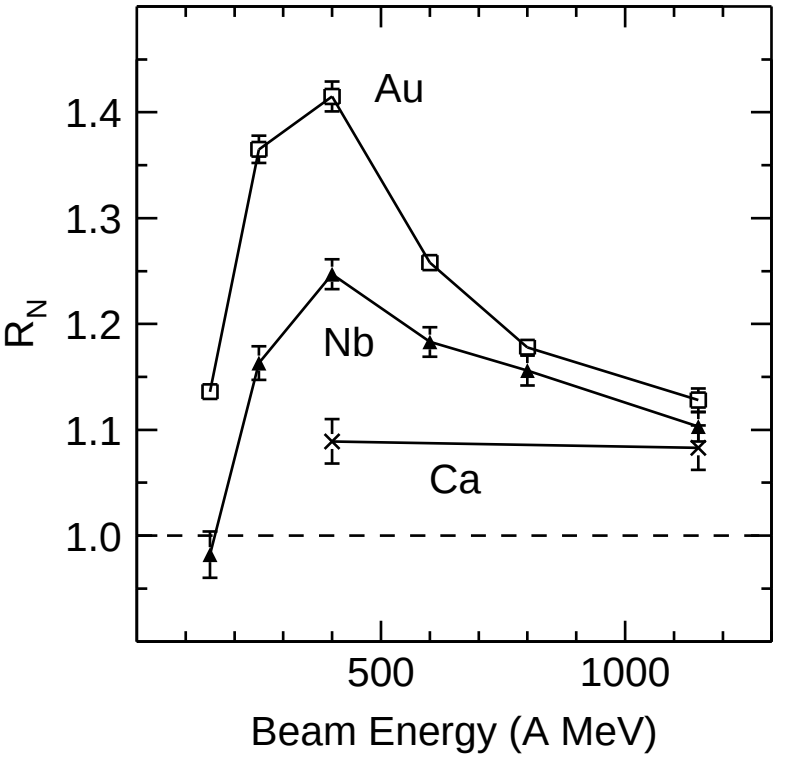

Figure 7 Excitation functions of the squeeze-out ratio for symmetric systems.

dependence from in-plane emission was speculated upon. However, comparing Figure 7 with Figure 4, the energy dependence has a similar form, since now in both cases dimensionless quantities are compared. This indicates again that both forms of flow do not scale as expected from ideal hydrodynamics.

Out-of-plane emission has been measured for a large range of energies from GANIL (126, 155) up to the highest Bevalac/SIS energies, and for protons and composite particles as well as for neutrons (156). The onset of the effect can be observed in Au+Au collisions at 100*A* MeV (157) where the second moment with a positive coefficient a_2 is seen for central collisions while peripheral collisions clearly show preferred in-plane emission (a_2 negative). This is the remnant of the rotational pattern typical for deep inelastic reactions. Determination of the reaction plane in a way that minimizes dispersion effects (26) is essential. This allows a better quantitative measure to be obtained at very large impact parameters, where other methods to determine the reaction plane diverge (24).

The KAOS Collaboration (158) has measured out-of-plane emission of protons and light composite fragments in Bi+Bi reactions at several energies with a spectrometer and has determined the reaction plane with the transverse-momentum method with the help of a hodoscope (159), in the spirit of Elaasar et al (47). This method allows flow measurements to be performed with relatively small effort and without covering the 4π solid angle, but does not allow the event to be rotated into the flow-tensor coordinate system, where out-of-plane emission is maximized (24). A strong effect is observed for protons. The composite fragments show an enhancement of the flow effect that is proportional to the particle mass (36, 148, 160).

A detailed comparison of neutrons and protons shows that R_N is the same for both particles (50, 156). Thus Coulomb effects do not play a role. Lambrecht et al also show that R_N is independent of energy (between 400A and 800A MeV) for neutrons in a fixed transverse momentum bin where the bin is scaled with the projectile momentum (50). This indicates that dynamics play an important role not revealed by the momentum integrated data.

An interesting new look at out-of-plane emission has been developed by the EOS Collaboration (161). Au+Au reactions at 600A MeV have been analyzed in the reference frame of the flow ellipsoid. The authors have analyzed the transverse mass, $m_\perp$, and rapidity, y, distributions of the particles emitted into mid-rapidity ($|y| < 0.4$) with a model where a radial flow velocity is superimposed on a locally thermalized velocity distribution (148, 162). The local temperature parameter, T, and the mean radial-flow velocity, β_f, were free parameters. Instead of fitting the emitted particles globally, as discussed in Section 5, in this case the spectra have been fitted for particles emitted into small bins in the azimuthal angle Φ' relative to the reaction plane. In Figure 8 the fitted values for β_f and T of $A = 2$ particles are shown as a function of emission angle relative to the reaction plane, Φ', for three different multiplicity bins. The lower panels show that for all multiplicities the apparent temperature is independent of the azimuthal angle, whereas the flow velocity in the top panel shows a modulation with maxima at 90° and 270° that can be described by $\beta(\Phi') = \beta_0 - \Delta\beta \cos(2\Phi')$. The KAOS Collaboration has performed a similar analysis (158).

The data suggest an interesting interpretation. Mid-rapidity emission occurs from a source with a constant apparent temperature. The out-of-plane emission shows a larger flow velocity since this is the direction where spectator remnants do not hinder the emission, hence the term in-plane retardation chosen by Wang et al (161). A larger flow velocity out-of-plane also could explain why the squeeze-out effect depends on the transverse momentum or the transverse mass of the emitted particles (50, 158, 163, 164). Wang et al also showed that coalescence can account for the increase of R_N with fragment mass.

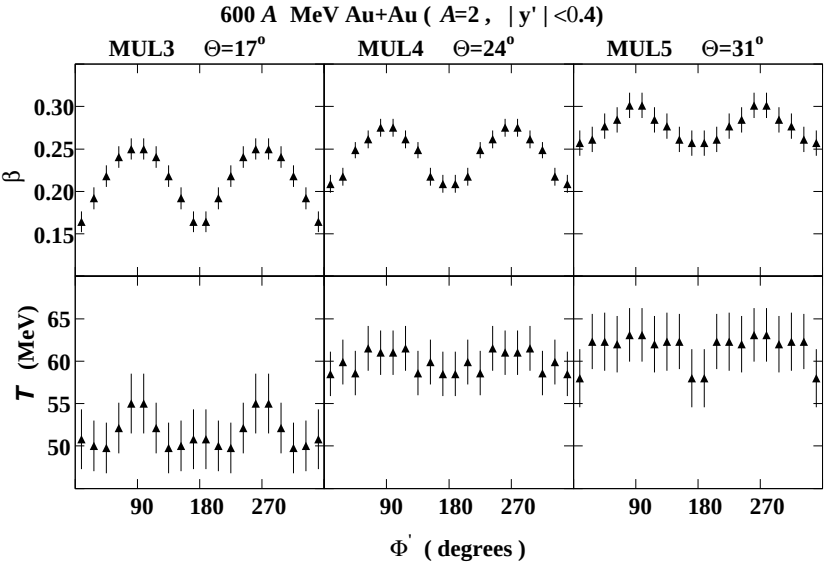

Figure 8 Values for the expansion velocity, β, and the temperature parameter, T, obtained from fits of the $A = 2$ spectra to the blast wave model as a function of the emission angle relative to the reaction plane, Φ'. The data for $\Phi' > 90^\circ$ were generated using reflection symmetry.

Theoretically, the most interesting feature is that the squeeze-out ratio appears to be very sensitive to some of the parameters of the equation of state. This was demonstrated by Hartnack et al (165, 166). A comparison of the 400*A* MeV Plastic Ball data (154) with QMD calculations shows that the data favor a soft equation of state. The difference in R_N is up to 25% for soft and hard equations of state, respectively. In addition, Hartnack et al demonstrate that out-of-plane emission is a collective effect that depends linearly on the mass of the colliding system. The EOS study (161) also confirms that the effect is sensitive to the EoS. In this case, comparison to QMD calculations (76, 167) shows that $\Delta\beta$, the variation of the flow velocity with the emission angle relative to the reaction plane, is most sensitive to K and that a hard EoS seems to better reproduce the 600*A* MeV data. However, overall agreement between data and models is not yet good enough and systematic enough to come to a firm conclusion (161). The apparent contradictions between different comparisons as far as the EoS is concerned could be an effect of energy dependence. This is supported by equally weak evidence in Reference 52.

The Miniball data (157) at 100, 200, and 400*A* MeV can be reproduced best by BUU calculations (168) with reduced in-medium cross sections $\sigma_{NN} = 0.8\sigma_{\text{free}}$,

but the dependence on K is not conclusive, partly for experimental reasons and because momentum-independent interactions were used. The BUU calculations also reproduce the transition from in-plane to out-of-plane preferred emission as a function of impact parameter. Cascade calculations do not reproduce the data. The energy dependence is wrong and at 250 and 400A MeV R_N is too small, in agreement with earlier findings that the intranuclear cascade does not show enough flow (77).

Danielewicz (168) has associated the sensitivity of the out-of-plane flow signal to the EoS semiquantitatively with a delay in the start of the longitudinal expansion compared to transverse (7). This delay was directly connected with the velocity of sound in the heated and compressed matter, which is larger for a harder EoS. Viscosity also influences this delay as it determines the width of the shock profile. This interpretation, in line with Wang et al (161), implies a purely *dynamic* origin of the effect. A different or additional explanation could be shadowing (see next section) caused by the presence of cold spectator matter. It was proposed (168) to resolve this ambiguity by studying azimuthal distributions in planes with different orientations with respect to spectator pieces. An alternative is to select very central (spectator-free) collisions and to study *polar* angular dependences of yields, spectral shapes, and kinetic energies. If dynamics is dominant, squeeze-out should lead to 90° (polar, azimuthally symmetric) peaking. A dramatic effect of this kind has not been seen so far (60, 148, 169).

4.2 *Flow of Produced Particles*

Recent experiments at GSI have shown an enhanced out-of-plane emission of charged (159, 170) and neutral pions (164, 171). The π^0 were observed with the TAPS photon spectrometer (172) and a forward wall was used to determine the reaction plane. In 1A GeV Au+Au reactions (164), ratios of $R_N = 9$ could be observed with an extreme momentum cut of 1 GeV/c. A dramatic effect on the pion spectra was measured as well. Figure 9 shows representative data for the ratio R_N (corrected for finite number fluctuations). These data were obtained by the KAOS Collaboration (170) using a spectrometer (173) for Bi+Bi at 400, 700 and 1000A MeV. An intermediate impact parameter was selected via cuts on the multiplicity distribution for charged particles in the laboratory polar angle range of 12 to 48°. Again, the out-of-plane enhancement rises with the transverse momentum, p_t. We have performed a least-squares fit with a quadratic dependence to the data at 700A MeV and then made a scaling prediction for the lower and higher energies (solid lines in Figure 9). One can see that scaling holds, except at the highest incident energy where the high p_t data level off for $p_t > 400$ MeV/c.

The KAOS Collaboration showed as well that there was no significant difference between π^+ and π^- (170), that there was only a weak hint that the

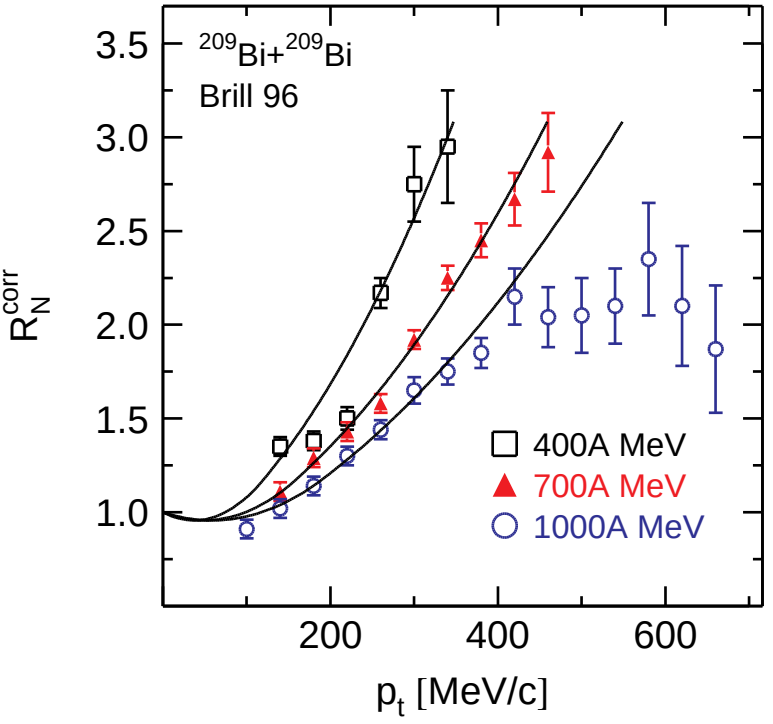

Figure 9 Ratio R_N for pions as a function of the transverse momentum in the reaction Bi+Bi at 400, 700 and 1000*A* MeV. The lines are explained in the text. After Brill et al (170).

squeeze-out was larger for more peripheral collisions, and that the effect was comparable in size to that found for the protons (158), *if one compares the data at the same kinetic energy*, rather than at the same p_t.

Microscopic model calculations of the azimuthal distributions of pions have been performed in the framework of BUU (104, 108, 174) and of QMD (103, 110, 163). As was discussed in connection with the in-plane asymmetries (Section 3.2), the transport theoretical investigations suggest that the apparent pion "flow" is less dynamical in origin (i.e. caused by pressure gradients), but rather is correlated with rescatterings and absorption on spectator matter. Calculations for 1*A* GeV correctly predict an out-of-plane effect for semi-central reactions (104, 163), but the BUU calculation (104) strongly underestimates R_N at all p_t values, while the QMD model (163) predicts strong Coulomb effects, not seen so clearly in the experimental R_N ratios (170), but seen in the pion spectra (175). According to Bass et al (163), the π^+ undergo an enhanced

repulsive out-of-plane push relative to their negative counterparts. In contrast to "squeeze-out" of baryonic matter, the out-of-plane enhancement of pion emission is predicted to grow *monotonically* with impact parameter (calculations up to $b/b_{max} = 0.7$ were presented in References 104, 163), again suggesting the importance of spectator matter. More high-statistics experimental data are required to test this prediction. A potentially interesting finding (163) is the predicted influence of the mean nucleon field, including its momentum dependence, on the details of the pionic out-of-plane emission, such as the impact-parameter dependence. In general one can conclude that a fully quantitative description of the present data has not been achieved and that more systematic data (including peripheral collisions) are needed.

5. RADIAL FLOW

5.1 *The Data*

Experimental evidence for the existence of radial flow is based on two phenomena observed in *central* collisions: (*a*) kinetic energy spectra of identified particles that do not show the characteristic Boltzmann-like shape expected for thermal emission, but rather a shoulder arm (176), and (*b*) a quasilinear dependence of the average kinetic energy on the mass or charge of the emitted fragment. Both these features are incompatible with the thermal model, where all emitted particles should have the same average energy.

It is common for radial-flow analyses either to achieve excellent centrality (less than 2% of the geometric cross section) or to limit the data to 90° in the c.m., where contamination from directed flow is small. The full three-dimensional topology of the events in velocity space needs to be carefully inspected in order to see if a well-defined source exists that would justify applying concepts of radially expanding matter. In addition, it is important to establish the size of the source and the relative importance of transverse and longitudinal flow.

Au+Au collisions have been investigated over a large energy range (60, 148, 160, 177–180). In particular, the EOS Collaboration (148) has measured energy spectra of isotope-separated charge one and two particles emitted around 90° in the c.m. without a transverse-momentum cutoff (181). Radial flow in central collisions was studied with the blast-wave formalism (162). In this model, the energy distribution in the center of mass for particles emitted from a thermally equilibrated, radially expanding source (characterized by a temperature, T, and a mean radial flow velocity, β_f) is given by the functional form (162)

$$\frac{dN}{dEd\Omega} \sim pe^{-\gamma_f E/T}\left\{\frac{\sinh\alpha}{\alpha}(\gamma_f E + T) - T\cosh\alpha\right\}, \qquad 8.$$

where E and p are the total energy and momentum of the particle in the center

of mass, $\gamma_f = (1 - \beta_f^2)^{-1/2}$, and $\alpha = \gamma_f \beta_f p/T$. The concept of a single flow velocity is quite simplistic, but it provides a useful way to parametrize the data and identify important components in the decay of the excited system. The parameters T and β_f have been extracted by fitting Equation 8 to the energy spectra measured at $\theta_{cm} = 90^\circ \pm 15^\circ$.

Figure 10 shows kinetic-energy spectra for protons, deuterons, tritons, ^{3}He, and α particles for the reaction Au+Au at 1.0*A* GeV. The data (circles) are from the most central events as selected by the charged particle multiplicity. Also shown are fits with Equation 8. Solid lines indicate a simultaneous fit to all spectra, excluding the protons, by varying β_f and *T*. A good overall fit is obtained, with a χ^2/ν on the order of unity. Dashed lines represent the fits for a purely thermal model, that is $\beta_f = 0$. The spectra are not as well reproduced, especially for the heavier fragments. Such behavior is observed at

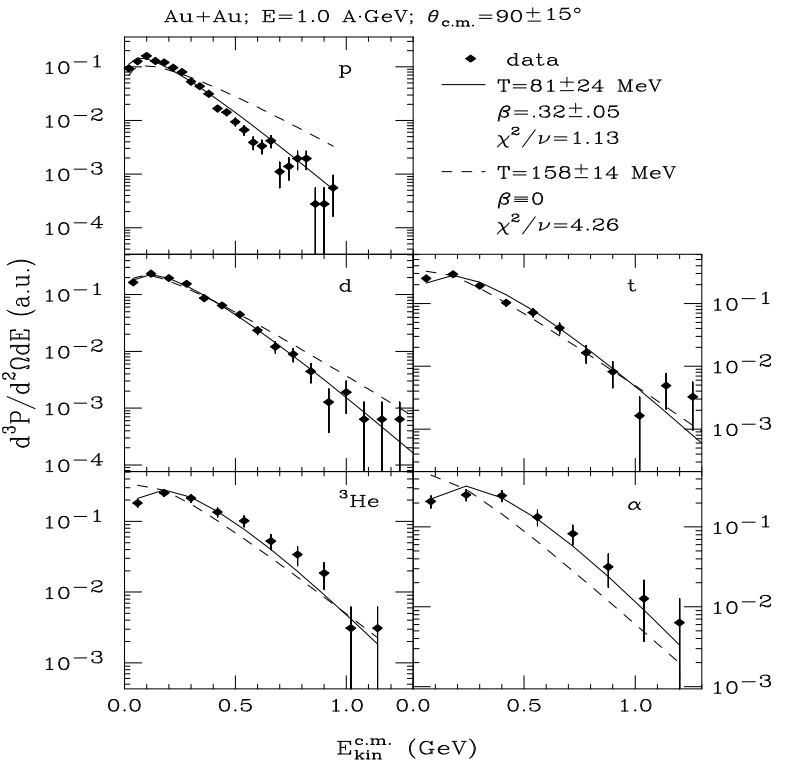

Figure 10 Energy spectra for light fragments emitted into $\theta_{cm} = 90^\circ \pm 15^\circ$. Fits with a radially expanding thermal source (*solid lines*), and a purely thermal source (*dashed lines*) are also shown.

all bombarding energies. The deduced collective radial flow is quite high: for alpha particles (deuterons) it represents 60% (45%) of their kinetic energy.

When spectra for a given fragment type (d, t, ^{3}He, α) are fitted individually, the extracted temperature and flow values are consistent with the values obtained by the simultaneous fit to all particle types. However, fit parameters for the protons deviate from the parameters for the heavier fragments. At all bombarding energies, proton spectra consistently yield a lower temperature and a larger flow parameter. This can be qualitatively understood (148) in terms of distortions of the proton spectrum due to baryonic (e.g. Δ) and nuclear (e.g. ^{5}Li) resonance decay.

For sufficiently central collisions, the analysis of the EOS data showed also that the flow measured at 90° in the center-of-mass system has the same value at other c.m. angles, i.e. that the flow has a radial shape. As shown in Section 4, the method could also be extended to intermediate impact parameters provided the analysis is done in the flow-axis system.

For a more limited energy range (100 to 250A MeV) isotope-separated light particle ($Z = 1$–2) spectra at 90° c.m. have also been analyzed by the FOPI Collaboration (178). The nuclear flow (see below) was deduced primarily from the mass dependence of the average kinetic energies of the hydrogen isotopes (p, d, t). To compare with the EOS data, an estimate of the Coulomb flow (common to the three hydrogen isotopes) must be added.

Taking advantage of the high sensitivity of intermediate-mass fragments (IMF, $Z > 2$) to flow, the FOPI Collaboration has made detailed investigations of IMF spectra and yields at 150, 250 and 400A MeV incident energies (160, 179, 60). For these fragments the masses were derived from the measured charges assuming $A = 2Z$. Very central events (about 1% of the geometrical cross section) were selected by requiring both high transverse energies and low directivity (Equation 4). The topology of these events is isotropic within about 20% (60, 169). Figure 11 shows the mean kinetic energy per fragment $\langle E_{kin} \rangle$ as a function of the fragment mass for the example of Au+Au collisions at 250A MeV (60, 179). The strictly linear increase of the mean kinetic energy as a function of mass has been taken as the first convincing evidence for the existence of large (radial) collective flow (160).

The data for the full measured phase space (excluding charge one particles) were analyzed with a radial expansion model (60) that assumes a common freeze-out temperature as was done in the EOS analysis (148). The total collective (flow) energy and thermal energy (and hence the temperature) were constrained by energy conservation. For the flow a more general Ansatz was used in the sense that a weighted integral $\int \Phi(\beta_f) n(\beta_f) \beta_f^2 d\beta_f$ over spectra $\Phi(\beta_f)$ of the type represented by Equation 8 was allowed for. In Figure 12 the rapidity distributions of heavy fragments (with a scaled transverse four-

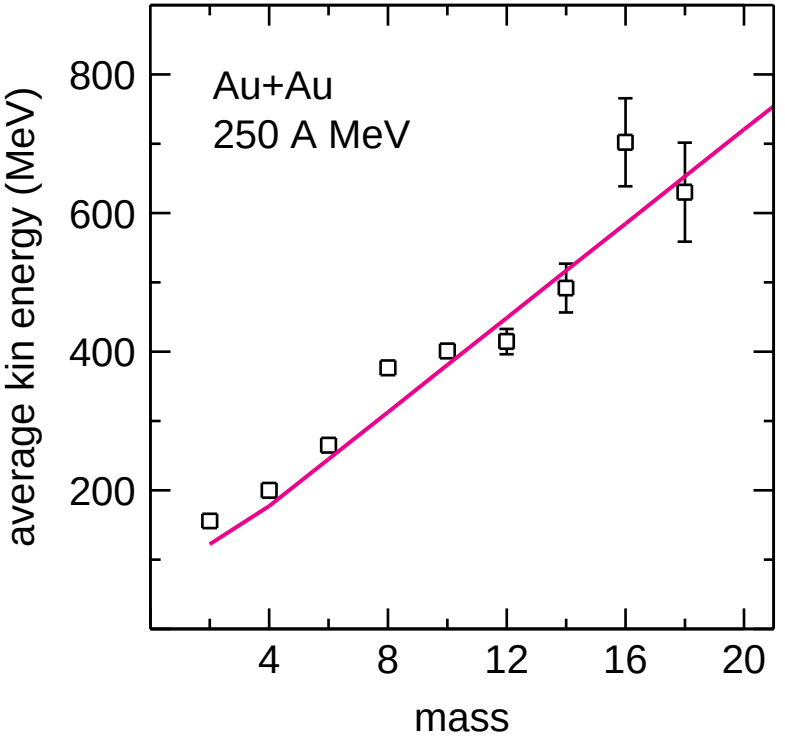

Figure 11 Average kinetic energy as function of mass in the polar angle range $25 - 45^{\circ}$ for Au+Au at 250*A* MeV. The line represents a fit to the full measured phase space with a radial expansion model using Woods-Saxon flow velocity profiles.

velocity cut $u_t < 0.6$) are shown to be sensitive to the assumed shape of the flow velocity profile $n(\beta_f)$. Both a δ-function profile, or "shell" (i.e. a single flow velocity, Equation 8) and a "box" profile [i.e. $n(\beta_f)$ is constant for $\beta_f < \beta_{fmax}$ and zero otherwise] fail to accurately follow the data. The latter are reproduced only if the sharp cut-off (Box) assumption is released by allowing for a diffuse Woods-Saxon (WS) distribution (see Reference 60 for details). In the analysis it was found that only heavy (IMF) fragments were sensitive to details of the flow profile. More complex flow profiles tend to require smaller temperatures and hence allow higher radial flow by energy conservation, which was used as a constraint in the analysis (60). However, the flow profile does not enter into the analysis if average kinetic energies as a function of mass are available, provided the one-temperature concept can be used (60, 178). The

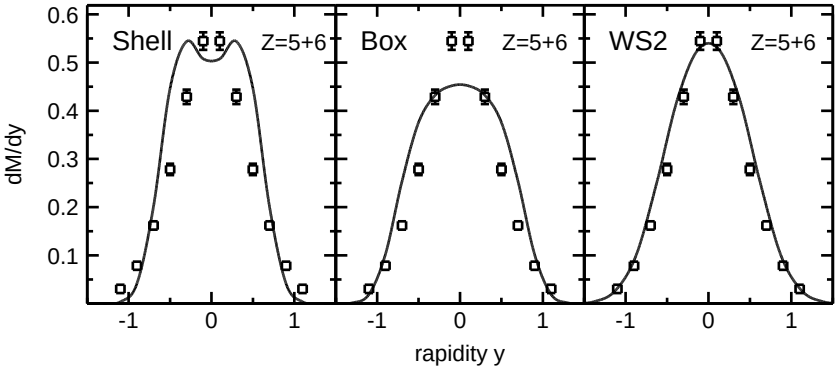

Figure 12 Measured rapidity distributions of fragments with nuclear charge $Z = 5$ or 6 in central Au+Au collisions at 250*A* MeV. The data (symbols) are compared with global fits using the blast model with flow profiles shell, box, and WS. A scaled transverse 4-velocity cut $u_t < 0.6$ was made.

solid line for the average kinetic energies in Figure 11 was obtained with the WS flow profile that also reproduces the *shapes* of the spectra. From the analysis in Reference 60 it was found that the total flow energy represents about 60% of the available outgoing total kinetic energy.

The compounded data for average radial-flow velocities, extending from 100*A* MeV all the way up to 1150*A* MeV, are plotted in Figure 13. The data, based primarily on the analysis of heavier-mass fragments (IMF) (60, 177), are joined by a smooth curve that has been obtained by a linear fit of the associated collective *energies* as a function of the incident energy. The figure also contains a horizontal band reflecting the (model-dependent) estimate of radial flow for a pure Coulomb explosion. Where a comparison is possible, i.e. at beam energies $\leq$400*A* MeV, the flow values obtained from light charged particles (LCP) are lower. As noted earlier, this may be a consequence of the more complex flow profiles used in the analyses (60) of the heavy cluster data or, alternatively, may result from the influence of sequential decay on the spectra.

An increasing set of data now exists for energies close to or below 100*A* MeV. Possible system-size dependencies and the quest for the mechanism that causes the onset of radial flow are at the center of interest here. These data are difficult to present in a common frame. As before, analyses tend to separate out a thermal and a collective component. Beyond that, many authors try to subtract with the help of event simulations the "Coulomb" flow, (E_f^C or β_f^C), which becomes at low energy an important background to the more interesting "nuclear" flow (flow beyond Coulomb) (E_f^N or β_f^N). Another complication, clearly evident in most of these lower-energy data, is the fact that the kinetic energy rises with

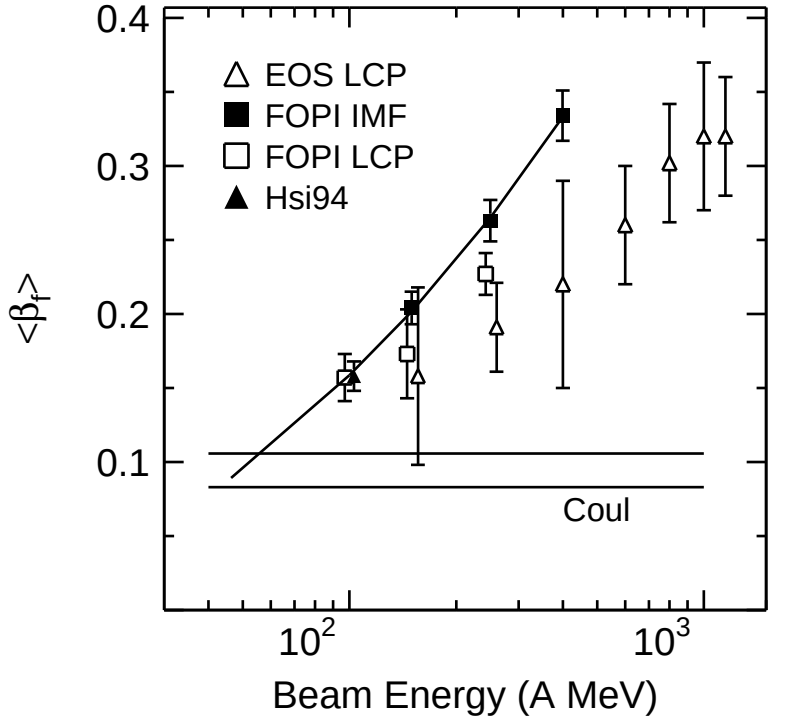

Figure 13 Excitation function of the radial flow velocity for Au+Au.

fragment size only for relatively light fragments, but then tends to decrease again for heavier fragments (177, 182). Finally, a third complication, which is of increasing importance as the energy and the system size are lowered, is the fact that the velocity space topology even for very central events shows rather strong deviations from sphericity.

Steckmeyer et al (183), studying the ^{64}Zr+Ti reaction in the energy range of 35 to 79*A* MeV, identified a fast "quasiprojectile" source even in the most central collisions ($b/b_{max} < 0.22$). A maximum excitation energy of 12*A* MeV (at 79*A* MeV incident energy) was determined with a caloric method. Then, looking at the average kinetic energies of fragments with $Z = 2$–9 *in the frame of the quasiprojectile*, where the topology was found to be isotropic, a radial flow of $(2.3 \pm 0.4)A$ MeV beyond the Coulomb flow was extracted.

A very similar analysis (184) was performed on ^{36}Ar+^{27}Al collisions between 55 and 95*A* MeV. The extra radial flow was found to gradually decrease to zero

as the excitation energy reaches values between 5 and 6*A* MeV, which could be interpreted as threshold value for thermally-induced expansive flow.

With inverse kinematics the fragmentation of the heavy projectile spectator of Au+C reactions at 1*A* GeV has been investigated (185). The total transverse kinetic energy of the emitted fragments (after separating fragments from the prompt stage of the reaction) is separated into a thermal, a Coulomb, and a collective component. In this case the temperature is determined from the yield of light isotopes (186). For events with very low multiplicity (low temperature) the collective component is very small, but it increases with fragment multiplicity and reaches up to 50% of the total available energy. It should be mentioned that such an interpretation is not unique and that the effects are very small. Compression is very unlikely to be the cause of this type of collective expansion; it looks as if thermal pressure is creating the collective motion.

Pak et al (187) studied *transverse* kinetic energies, E_{kt}, as a function of angle and impact parameter for ^{40}Ar+^{45}Sc at 35 to 115*A* MeV. The authors deduced a nuclear flow energy of about 7*A* MeV for ^{9}Be fragments at 115*A* MeV, which would be compatible with the Au+Au data, although the system here is much smaller. No detailed discussion of the topology was done, but the data indicate that the transverse energies at angles other than 90° were substantially lower (by about half) than expected from spherical expansion.

Emulsion studies (188–190), which were among the first to give evidence for radial flow, were devoted to reactions induced by ^{12}C, ^{16}O, ^{36}Ar and ^{84}Kr on AgBr emulsions at incident energies of 60 to 220*A* MeV. Central collisions were selected via multiplicity and with use of a flow-tensor analysis. Studying average kinetic energies as a function of Z_f, Barz et al (188) found a flat trend for ^{16}O induced reactions at $(20 \pm 10)A$ MeV, while they extracted a value $E_f = 3.2A$ MeV for ^{36}Ar+AgBr at $(65 \pm 15)A$ MeV and $Z_f = 1$ to 13.

Heuer et al (191) have derived a radial flow energy $E_f^N = 3.5A$ MeV for the system ^{32}S+^{27}Al at 37.5*A* MeV. The value found for the flow energy would correspond to 38% of the c.m. energy. Radial flow was determined by requiring the simulation to reproduce the measured two-fragment correlation function and the distribution of the squared momenta of the heaviest fragment (typically $Z_f = 8$) while accounting for the total available energy.

Very recent data obtained at the GANIL accelerator have been summarized by Borderie (192). Briefly, a radial flow, E_f, growing from about 0.5 to 2*A* MeV, was extracted from central collisions of ^{129}Xe+^{119}Sn (182) when the incident energy was varied from 32 to 50*A* MeV. Together with the reconstructed apparent excitation energies, this would set the threshold for the phenomena between 5 and 6*A* MeV, in agreement with Jeong et al (184) for a much lighter system. Values of E_f^N close to 1*A* MeV were shown in the survey (192) for

Pb+Au at 29 and Gd+U at 36*A* MeV. Virtually no extra flow was seen in Ar+Ni at 55*A* MeV, in apparent contradiction to other work (130, 183, 184, 191).

Data for Au on Au at 35*A* MeV are available (180). The analysis with the statistical multifragmentation model (193) yielded no flow or a flow of 0.8*A* MeV, depending on the assumptions made.

Despite some inconsistencies in the data it can be concluded that radial flow beyond the Coulomb flow starts to be seen around 5 to 6*A* MeV excitation. It has a rather small system size dependence if quantized in flow energy *per nucleon*.

5.2 *Theoretical Considerations*

In the fireball model (194, 195), breakup of the hot equilibrated system into a free-streaming system occurs immediately after its formation. Hence, in this model the emitted particles are expected to exhibit a purely thermal distribution. Siemens and Rasmussen (162) pointed out that the observed shapes of proton and pion spectra in central reactions of Ar+KCl at 800*A* MeV were not compatible with this assumption and introduced the so-called blast-wave picture, in which it was assumed that an isotropic hydrodynamical expansion that converted part of the initial thermal energy into radial flow took place before the final breakup. Assuming a single breakup flow velocity and temperature, they could reproduce the spectra, in particular the bending of the proton cross sections for c.m. energies below 200*A* MeV. In the model, the phenomenon of convex or shoulder-arm spectra is expected to be most pronounced if the ratio of the flow energy to the thermal energy at freeze-out is high. This model was also used in the analysis of the EoS data (148) (see Figure 10).

A calculation of the spherical expansion within the framework of relativistic hydrodynamics (196) shows that while the constant temperature assumption is justifiable, the flow velocity is not constant. Rather, it increases nearly linearly with the breakup radius. Besides the initial conditions of density and temperature (fixed by the Rankine-Hugoniot equation) the breakup and flow were shown to be also influenced by viscosity. In this calculation, however, the bending of the proton spectrum could not be reproduced because the low flow velocities for the central fluid elements tended to fill up the low-energy part of the spectrum. It was speculated that in the data this part was depleted by enhanced formation of heavier clusters in the central region. In the model, fluid elements that reach a given breakup density (chosen to be $0.75\rho_0$) while the system expands are switched to free streaming, and cease to participate actively (196). The process starts in the surface region that reaches the breakup condition earliest and as time elapses it gradually reaches the central elements.

Near-constant temperature at freeze-out (196) lends some justification to the many experimental analyses using the one-temperature assumption. If one

subtracts the collective energy from the available energy and interprets the remaining energy as thermal energy, as implied by the radial expansion model, one can make an important check on the assumption of chemical equilibrium at freeze-out using statistical models (193, 197, 198). An assumption is that the flow has no back-influence on particle formation or production other than by removing locally available energy. For large flow velocities this assumption may be unrealistic (199). The production of heavy clusters $Z > 5$ in Au+Au collisions is severely underestimated when such statistical concepts are applied (60). To what degree this is a genuine nonequilibrium effect, or just a failure of the (low-density) statistical models to correctly describe the clusterization probability, needs to be clarified. Similar difficulties in simultaneously accounting for the energies and yields of the *light* particles (Au+Au 100–250*A* MeV) were encountered elsewhere (178). A consistent check of the chemical equilibrium hypothesis (under the constraints of the flow information and energy conservation) at the higher end of the SIS/Bevalac energy range (0.6–2.0*A* GeV) has yet to be done (see Section 6 for AGS and CERN energies). It is however clear that radial flow and the thermo-chemical model are strongly connected. As pointed out in a detailed theoretical study (168), the presence of collective flow is highly relevant in attempts to understand pion production quantitatively, requiring at least partial reassessment of earlier attempts (200, 81) to directly connect pion yields to the EoS.

Historically, earlier work by Bondorf et al (201) studying the isotropic expansion of an ideal gas into vacuum made use of self-similar solutions to the problem in which the local flow velocity, β_f, exactly follows the Hubble-like relation

$$\beta_f = Hr, \qquad 9.$$

at all times and in which all observables (density, temperature, entropy, pressure, flow energy, etc.) are functions of the scaled radius r/R where R is the time-dependent outer radius of the expanding system. Such self-similar solutions require certain initial conditions, however.

The basic concepts of the model (201) were applied to Au+Au data at 250*A* MeV (179). With three adjustable parameters (essentially the initial central density, a density profile shape parameter (201), and a variable freeze-out condition) a good account of the kinetic energies of fragments with $Z = 2$–6 could be made. The local freeze-out temperatures were used as input for a statistical multifragmentation model (198). For $Z = 1$–6 the yields (adjusted at $Z = 4$) could be reproduced within a factor of 2 to 3. However, post-explosion decay, which strongly modifies the ratios for $Z = 1$ to $Z > 5$ clusters (60), was not taken into account. An interesting feature was that the initial configuration as constrained by the fit to the data tended to have smaller specific entropy in the

central region, as opposed to the surface region, leading (as the expansion is isentropic for each fluid cell) to heavier fragments being formed deeper inside (and later) and hence having somewhat less flow energy than light particles. In the data, this effect is increasingly important at energies $\leq 100A$ MeV (177, 182). More naively, one may argue that heavier fragments must be formed further inside for geometrical reasons.

It is instructive to make a simple estimate of the maximum achievable density and pressure by solving the relativistic Rankine-Hugoniot-Taub (RHT) equation:

$$W^2 - W_0^2 = P\left(\frac{W_0}{\rho_0} - \frac{W}{\rho}\right), \qquad 10.$$

where

$$W = W_0 + W_c + W_T$$

$$P = P_c + P_T$$

$$P_c = \rho^2 \frac{dW_c}{d\rho}$$

$$P_T = \alpha \rho W_T.$$

The energy per nucleon W contains besides the ground state energy W_0, the compressional energy W_c ("cold EoS") and the thermal energy ("thermal" EoS) to which correspond, respectively, the compressional ("mean field") pressure P_c and the thermal ("kinetic") pressure P_T. For a nonrelativistic noninteracting Fermi gas the coefficient $\alpha = 2/3$.

Figure 14 shows the resulting density achieved in the stopped (shocked) matter for different cold EoS, each in combination with the noninteracting Fermi gas for the thermal EoS. The curves marked S (soft) and H (hard) correspond to two EoS frequently used in QMD (76) and BUU (73) calculations. The "cold" compression energy needed to achieve twice saturation density, $K2$, is $10A$ MeV for S, $22.4A$ MeV for H. For reference the pure Fermi-gas case, FG, with $K2 = 0$ (supersoft), is also shown. Remarkably, this maximum density rises fastest at relatively low density, reaching values of $2\rho_0$ already around $100A$ MeV ($200A$ MeV) for the soft (hard) case.

Figure 14 also shows the ratio of total pressure to available energy. The differences, when varying the EoS, are not dramatic as has been discussed by Stöcker, Gyulassy, and Boguta (202), where it was concluded that a very high accuracy of flow and entropy measurements would be needed to deduce information on the cold EoS. It turns out that for a given incident energy, the conservation laws (energy, momentum, mass) that are the basis of the RHT equation severely limit the *total* pressure achieved. The small change of the

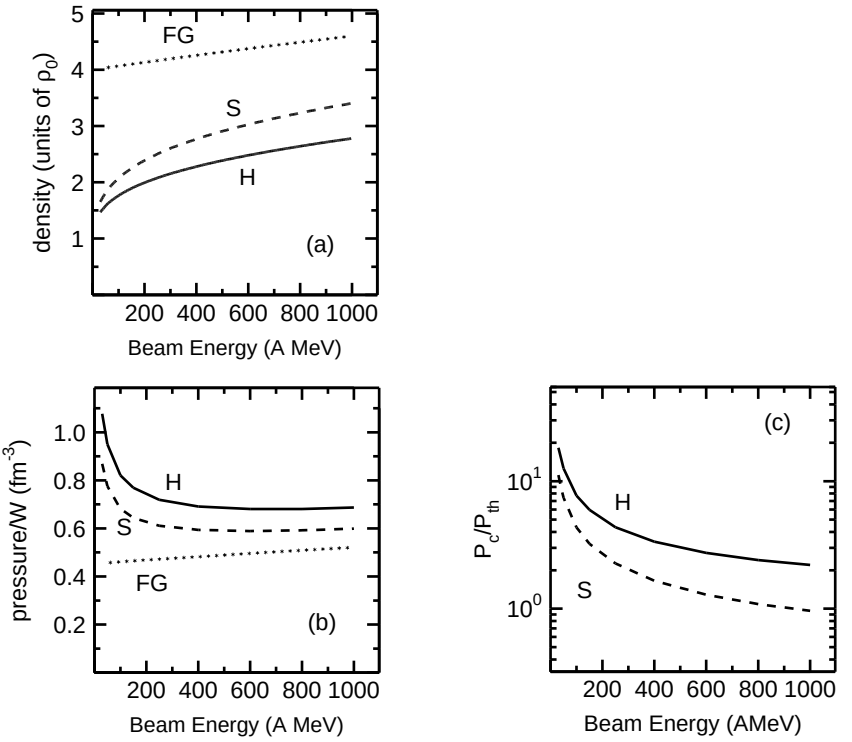

Figure 14 Rankine-Hugoniot-Taub shocks. The dependence on the incident energy is plotted for a Fermi gas (FG), a soft (S), and a hard (H) EoS. (*a*) Number density in the stopped zone; (*b*) ratio of pressure to c.o.m. energy; (*c*) ratio of compressional to thermal pressures.

total pressure with $K2$ might explain the relative insensitivity of radial flow found in microscopic calculations (60, 148, 203) at energies beyond 200*A* MeV.

Rather low incident energies were proposed to study the cold EoS (202). Indeed, a dramatic violation of the scaling properties occurs below 150*A* MeV. The Fermi gas pressure scales over the full energy range to within about 10%. The relative dynamical importance (at the beginning of the decompression) of cold versus thermal EoS, quantized by the ratio of corresponding pressures, is suggested in panel (*c*) of Figure 14: the *relative* compressional pressure is most important at low energies. Unfortunately, at these energies the *absolute* compression (energy) is also lowest.

In general it seems that the maximum densities predicted in microscopic transport calculations are systematically lower than the estimates from RHT, aside from the fact that they are only achieved for a brief time in a fraction of

the colliding system (168, 204–207). As a consequence, the possible connection between radial flow and the cold EoS should be weakened. One of the reasons for the lower densities may lie in partial thermalization at the time of maximal compression (204–207). In general, strongly momentum-dependent mean fields lead to a further lowering of the maximum density due to increased sideways deflection in the early stages of the collisions.

Concerning the observed onset of radial flow phenomena in systems excited to about 6*A* MeV (184, 192), it is unlikely that shock phenomena are responsible for this observation, although the condition that the projectile velocity be higher than the velocity of sound c_s is already fulfilled at rather low incident energies. Using the relation $c_s = \sqrt{K/9m_n}$ one obtains 10 to 20*A* MeV for $K =$ 180–360 MeV. It was shown that Pauli blocking effectively leads (for Au+Au at 200*A* MeV) to an increase of the mean free path of the nucleons from about 1 to 2.5 fm (206), a value that might be increased further if in-medium modifications (Pauli blocking of intermediate states) are taken into account (208). The blocking effect is likely to be even larger at still lower energy. The resulting large viscosity will tend to lead to delocalized shock fronts (68) or even to partial transparency. Antisymmetrized transport theory (209, 210) might be necessary to settle the question of viscosity at low energies. It appears that the onset of radial flow is more likely due to thermal pressure rather than compression-induced mean-field gradients. Further investigations appear necessary to reach a more definite conclusion. Determining nuclear viscosity via stopping studies is an important goal and prerequisite to understanding radial flow: viscosity limits the maximal density and influences the freeze-out condition.

6. AGS AND CERN ENERGIES

6.1 *Directed Flow*

Data are less abundant at AGS and CERN energies. At Bevalac/SIS energies, directed flow is a relatively small effect (energy in directed motion compared to the center-of-mass motion), i.e. the flow angle is small. Only specially designed experiments have a chance to measure such an effect. From the beginning of the CERN program, WA80 (211) [with the Plastic Ball (15) covering the target rapidity region], has had an azimuthally symmetric setup that is potentially capable of detecting directed flow. At the AGS experiment E814 (212) was built up to include two different calorimeters covering the participant and the target regions.

Directed flow at the AGS was first observed by the E877 Collaboration (213) in Au+Au collisions at 10*A* GeV. The experiment has nearly 4π calorimetric coverage. Directed flow could be identified by using a Fourier-expansion analysis of azimuthal distributions (214, 215) (analogous to Equation 3). An

azimuthal anisotropy anticorrelated in the forward and backward hemispheres and most pronounced at intermediate impact parameters could be clearly measured. The signal disappears for very peripheral and central collisions. In addition to the existence of a strong first moment, at mid-rapidity a nonzero second moment can be observed, but contrary to the squeeze-out at lower energies (154), the effect is in the reaction plane.

The same collaboration later succeeded in measuring the directed flow more precisely by adding silicon counters to the E877 setup (216) to measure the charged particle multiplicity. By combining the calorimetric and multiplicity information, the collaboration could separate between flow of nucleons and pions for an intermediate multiplicity bin (217). Pions show the shadowing effect, whereas a strong signal for the proton flow could be determined. If calculated with normalized rapidity, the slope has about the same value in this experiment as at 2*A* GeV. Given the rather indirect way this value was determined, it will be interesting to see how it will compare to the excitation function being measured by E895. Figure 15 shows how the new data point compares to the values measured at lower energy. The figure documents the rise and fall of sideflow. Note that the FOPI data, obtained with heavier clusters, were scaled down by a factor of 0.7 to remove the systematic difference with data from light charged particles (see Figure 4). The dashed line is an extrapolation from the AGS point, assuming the function $\langle p_x \rangle (y)$ to be the same at all energies. A preliminary point from E895 (218) lies below this curve.

At CERN energies the data are much more sparse. The WA80 Collaboration (219) has reported an azimuthal asymmetry in the target region, and recently NA49 (220) has reported an effect in the second moment ($a_2 \neq 0$) measured with the NA49 calorimeters in intermediate–impact-parameter events. This very interesting result needs further analysis. The collaboration attempts to see the effect reproduced via the analysis of the charged particles. Ollitrault predicts asymmetry as a sign of directed flow in Pb+Pb collisions (221).

Measurement of directed flow is interesting primarily because (model dependent) information about the equation of state of nuclear matter can be deduced. Compared to lower energies, the models are not as sophisticated and complete. Mean-field effects should be less important, but not negligible (222). UQMD calculations (223) predict a steady increase of the directed flow between 1 and 4*A* GeV if calculated with normalized rapidity, which would translate into a rather flat behavior in terms of values plotted in Figure 15. This does not agree with the data point at 10*A* GeV.

The proton and pion flow measured by E877 (217) has been compared with model calculations. ARC (72) calculations qualitatively agree with the data. Peilert's prediction for $\langle p_x/A \rangle$ is lower than the data (224), whereas other RQMD calculations (225) show better agreement, which seems to improve

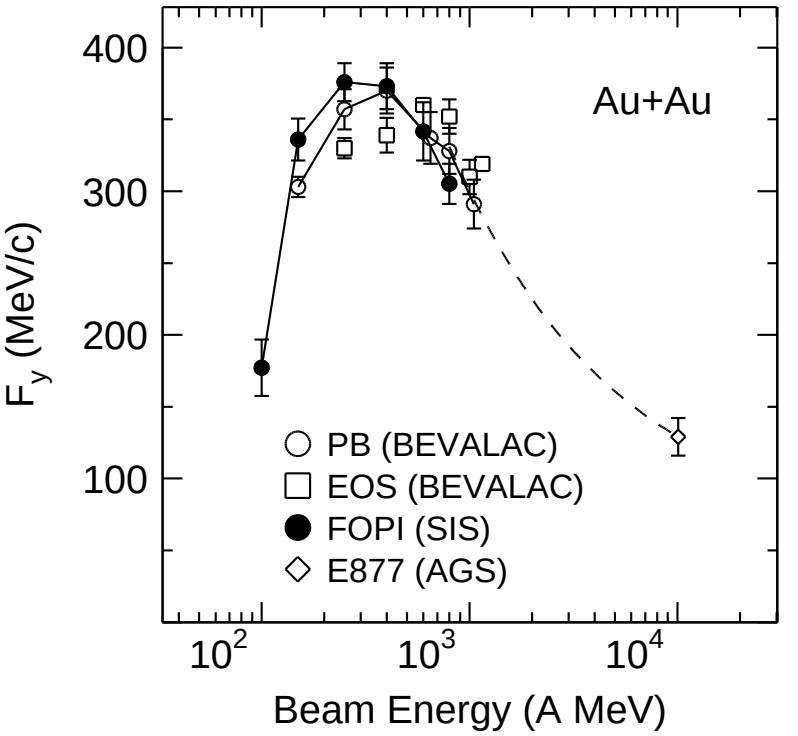

Figure 15 Sideflow excitation function for Au+Au.

by including mean-field effects (222, 226). In order to solve the question of whether mean-field effects still play a role at this energy, much more precise measurements (and detailed calculations) will be needed.

The second-moment effect in the azimuthal emission pattern can be used to distinguish between different expansion scenarios (227). Especially the transition from out-of-plane emission to in-plane preferred emission can be used to determine the strength of the early pressure (228).

The energy dependence of directed flow is expected to reveal changes that hot and dense matter might undergo. An expected effect is that at around 1*A* GeV the equation of state will soften due to the onset of copious particle and resonance production. New and exotic forms of matter should manifest themselves in a similar way (229). Production of a quark-gluon plasma also could lead to such effects. Hydrodynamic model calculations predict not only a signature in the pion multiplicity (230), but also a dramatic effect on the value of directed flow.

Hung and Shuryak (231) argue that the softest point in the EoS could be used as a way to find the QCD phase transition. Their hydrodynamic calculation shows that at this point the lifetime of the system is longest, which leads to other possible observables, e.g. by interferometry. Rischke has used an ideal relativistic 3+1-dimensional hydrodynamic model to calculate the directed flow for Au+Au collisions as a function of beam energy (232). With a hadron gas EoS, flow steadily decreases from the maximum at 2*A* GeV up to about 100*A* GeV. With a quark-gluon plasma EoS, the calculations predict an extended mixed phase. As a result of this, the flow will stall or at least be drastically reduced in the transition region. The flow value will have a well-pronounced minimum and might even become zero. At higher energies it will increase again until it reaches the hadron-gas value at around 100*A* GeV. Ideal hydrodynamics predicts the minimum at 6*A* GeV, in the middle of the AGS energy range, but the position of the minimum strongly depends on the model parameters, viscosity, and the choice of initial conditions.

Since the onset of new phases or new and exotic forms of matter is reflected in the equation of state, it is obvious that a study of the energy dependence of directed flow is rather promising. The E895 Collaboration (EOS) at the AGS (218) is bridging the gap between the highest AGS energy and the Bevalac/SIS energy range with a very detailed study. It will be most interesting to see those results. E895 should also be able to measure the transition of the second moment from preferred out-of-plane emission to in-plane emission.

6.2 *Radial Flow*

At energies around 1*A* GeV there is good experimental evidence that the three-dimensional collective expansion is in the form of radial (spherical) flow (148). At higher energies such a shape is not very probable. Lorentz contraction alone (10:1 at CERN energies) will lead to different expansion in longitudinal and transverse directions. It is convenient to separate longitudinal and transverse flow and to examine the experimental evidence and some of the theoretical considerations. Ultimately, we expect that we will be able to come to a unified description.

Longitudinal flow should manifest itself as a widening of the rapidity distributions (233). However, there is no way to distinguish (from those distributions alone) between longitudinal flow and partial transparency, known to be present at those energies (17). For the heavier systems measured at the AGS and SPS, the rapidity distributions tend to peak at mid-rapidity for protons and for produced particles (234–236). As an indication of the high density reached, microscopic models have to include mechanisms that go beyond the assumption of multiple binary hadron collisions with known cross sections in order to reproduce the peak at mid-rapidity (19). An analysis of the light systems measured

at the AGS, with ideal-gas thermodynamics with chemical equilibrium and strangeness conservation (237), gives a good fit to the rapidity distributions of the produced particles with a longitudinal mean flow velocity $\langle \beta_l \rangle = 0.52$.

Transverse flow has been conjectured from the study of particle spectra. Until recently, however, measurements have not been as complete and systematic as at lower energies. What is missing is a wide range of masses of the observed particles so that the mass dependence of the spectra can be analyzed.

The transverse-momentum spectra of hadrons measured in the early AGS and CERN experiments (light ions) have been analyzed by Lee, Heinz, and Schnedermann with an expanding fireball model (238). The authors find that the multitudes of different spectra from many different reactions are compatible with transverse flow on the order of $\beta_t = 0.4$ and a freeze-out temperature on the order of 110 MeV. Schnedermann, Sollfrank, and Heinz later performed a similar analysis (239) on the S+S data from CERN experiment NA35 (240). Again, the thermal model is consistent with the data, when some form of longitudinal flow is included. The light system, however, does not allow any conclusion about transverse flow.

The thermal analysis can be extended by including the assumption of chemical equilibrium and of a common chemical and thermal freeze-out (at the same temperature). This is a way to remove the ambiguity between temperature and flow velocity by fixing the temperature via the particle yields (237, 241).

A possibly clearer picture emerges from the analysis of the Pb+Pb data at 158*A* GeV. The NA44 Collaboration (235, 242) recently presented transverse mass spectra of pions, kaons, and protons. In this case, the slope parameter of the spectra clearly increased as a function of the particle mass. This behavior can be described by the assumption of a common freeze-out temperature and a common flow velocity. The temperature parameter seems to saturate at about 140 MeV (235) and the mean flow velocity reaches about 0.4. The E802 results with light ions (243) and with Au+Au reactions (236) lead to very similar conclusions.

An alternative view of the particle spectra measured by the CERN experiments has been presented recently by Leonidov et al (244). The authors describe the collisions by a superposition of isotropically decaying sources. The parameters are determined from *pp* and *pA* collisions. This leads to parameter-free predictions for nuclear collisions. Such predictions are in good agreement with the transverse mass spectra analyzed from Pb+Pb collisions (234). The authors conclude that the single-particle spectra require neither collective flow nor temperature increase (244). Other studies with an expanding source model also conclude that the freeze-out temperature is quite low (245). This needs extensive testing and comparison with all available data (235) before the issue can be settled.

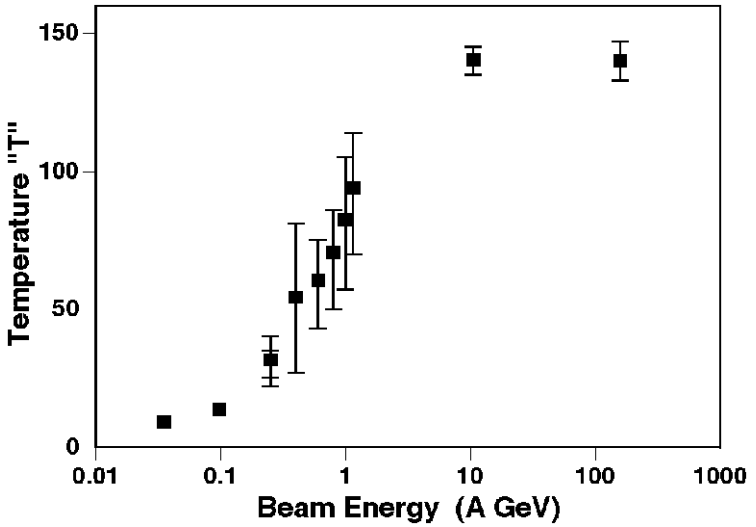

Figure 16 Values for the temperature parameter T as a function of beam energy.

An interesting picture emerges at all energies: for the heavy systems, transverse flow is an important part of the expansion dynamics. As a function of beam energy, the mean flow velocity increases and reaches about 0.4 at AGS energies. When extracted from the slope of the spectra, the apparent temperature gradually increases with energy as well and seems to saturate at around 140 MeV. This behavior is shown in Figure 16 (235, 246). It should be pointed out that realistic temperature values that are the same for all particles can only be obtained by taking collective expansion and resonance decay into account. The apparent saturation of the temperature indicates that additional energy no longer goes into heat, but rather into particle production. The question of whether or not we are close to a critical temperature is very interesting.

The simple assumptions of hydrodynamics are questioned by microscopic analyses. RQMD studies (226) indicate that the flow velocity of heavier particles is smaller than that of light particles. Also, the assumption of chemical equilibrium might not be justified. Sequential particle emission and a complicated freeze-out pattern are also the result of an analysis with a quark-gluon string model (247).

It is interesting to compare the effects of directed and transverse flow. Directed flow is established early on in the collision. It carries the memory of the collision geometry and thus is expected to carry information about the hot and dense state of the collision. Transverse flow, on the other hand, seems to

be characteristic of the expansion phase. In that respect, the magnitude of transverse flow is only one of the many quantities characterizing the freeze-out state, like temperature, chemical potential, entropy, etc. Thus the magnitude of the flow is very important in the attempt to reach a full thermodynamic or even thermodynamic and hadro-chemical description of the collisions and the freeze-out. The goal is to determine where the final state ends up in phase space (19). Such a determination could exclude, for example, a purely pionic equation of state in a hydrodynamical approach (248), or it could test, for example, if the freeze-out point lies close to the phase boundary for quark-gluon plasma formation (237, 241, 249).

7. SUMMARY AND OUTLOOK

The search for collective effects was a strong motivation for the early experiments. Understanding those effects continues to be an important part of the heavy-ion program. The appearance of collective effects can be taken as a sign that relatively few constituents (up to about 400 baryons in Au+Au collisions) reach a stage of high compression and high temperature. This is our only chance to study strongly interacting matter in the laboratory.

Different forms of collective flow have been observed from the threshold at low energies where the interplay between attractive and repulsive forces leads to interesting observables up to CERN energies where a large part of the energy available in the center-of-mass system is contained in radial flow.

In terms of energy, radial flow is the most prominent effect. Understanding radial flow is essential to determine the freeze-out temperature and the chemical properties of nuclear matter. The question of whether some form of equilibrium is reached, the concept of a common temperature for all fragments, and a common freeze-out will hold is far from being settled.

Sideflow has been studied in great detail. Its properties cannot (yet) be uniquely coupled to the parameters of the EoS. In models it depends too much on technical parameters and on the realistic description of the nucleus. We need to understand the dependence of flow on the energy and the transition from attractive to repulsive behavior. More experimental information on the transfer of energy from participants to spectators is needed.

Out-of-plane emission is restricted to energies below 10*A* GeV. This intriguing dynamical effect can help in the study of the role of shadowing and absorption. Out-of-plane emission seems to be quite sensitive to the EoS.

Hydrodynamic models have been used to make good qualitative predictions in all energy domains. It is obvious that the role of nonlocal equilibrium, momentum dependence, and corona effects needs to be investigated. While it may be interesting to describe the reaction with macroscopic concepts, it is essential to understand the processes microscopically. At energies below 1*A* GeV,

semiclassical transport models have been successful in describing the experimental observables. A long succession of experimental and theoretical progress has shown us that flow effects depend in a complicated way not only on the EoS but also on medium effects, and that a clean separation is very difficult. Only a complete (full-event) and systematic comparison with all the experimental observables will lead to more progress. Some studies seem to converge towards a model-dependent, soft equation of state, but a more conclusive result has to wait for more systematic comparisons over a large energy range. New theoretical developments towards a fully relativistic description of collisions and medium effects will help in this process. At the low-energy end, the role of proper antisymmetrization of the fermionic matter component will also have to be further explored.

ACKNOWLEDGMENTS

We would like to thank our colleagues from the FOPI and EOS Collaborations for interesting discussions and help with presenting the data. We have benefited from stimulating discussions with P Jacobs, D Keane, V Koch, MA Lisa, S Margetis, AM Poskanzer, G Rai, TJM Symons, and N Xu. This work was supported in part by the Director, Office of Energy Research, Office of High Energy and Nuclear Physics, Division of Nuclear Physics of the US Department of Energy under Contract DE-AC03-76SF00098.

Literature Cited

1. Landau LD, Lifshitz EM. *Fluid Mechanics.* London: Pergamon Press (1959).
2. Stöcker H, Greiner W. *Phys. Rep.* 137:277 (1986).
3. Clare RB, Strottman D. *Phys. Rep.* 141: 177 (1986).
4. Belenkij SZ, Landau LD. *Usp. Fiz. Nauk* 56:309 (1955); *Nuovo Cimento Suppl.* 3:15 (1956).
5. Glassgold AE, Heckrotte W, Watson KM. *Ann. Phys.* (NY) 6:1 (1959).
6. Chapline GF, et al. *Phys. Rev. D* 8:4302 (1973).
7. Scheid W, Müller H, Greiner W. *Phys. Rev. Lett.* 32:741 (1974).
8. Wong CY, Welton TA. *Phys. Lett. B* 34: 243 (1974).
9. Abul-Magd AY. *Phys. Rev. C* 12:343 (1975).
10. Sobel MI, Siemens PJ, Bethe HA. *Nucl. Phys.* A251:502 (1975).
11. Kitazoe Y, Sano M. *Prog. Theor. Phys.* 54:922 (1975); 54:1774 (1975); *Nuovo Cimento Lett.* 14:400 (1975); 14:407 (1975).
12. Gustafsson HÅ, et al. *Phys. Rev. Lett.* 52:1590 (1984).
13. Renfordt RE, et al. *Phys. Rev. Lett.* 53:763 (1984).
14. Ströbele H, et al. *Phys. Rev. C* 27:1349 (1983).
15. Baden A, et al. *Nucl. Instr. Meth.* 203:189 (1982).
16. Buchwald G, et al. *Phys. Rev. Lett.* 52:1594 (1984).
17. Stachel J, Young GR. *Annu. Rev. Nucl. Part. Sci.* 42:537 (1992).
18. Kahana SH, et al. *Annu. Rev. Nucl. Part. Sci.* 46:31 (1996).
19. Harris JW, Müller B. *Annu. Rev. Nucl. Part. Sci.* 46:71 (1996).
20. Braun-Munzinger P, Specht HJ, Stock R,

Stöcker H, eds., *Proc. Quark Matter 96. Nucl. Phys. A* 610 (1996).
21. Bertsch GF. *Phys. Rev. Lett.* 34:697 (1975).
22. Gyulassy M, Frankel KA, Stöcker H. *Phys. Lett. B* 110:185 (1982).
23. Cugnon J, L'Hôte D. *Nucl. Phys. A* 397:519 (1983).
24. Gutbrod HH, et al. *Phys. Rev. C* 42:640 (1990).
25. Danielewicz P, Odyniec G. *Phys. Lett. B* 157:146 (1985).
26. Danielewicz P, et al. *Phys. Rev. C* 38:120 (1988).
27. Gutbrod HH, et al. *Phys. Rev. Lett.* 37:667 (1976).
28. Balazs NL, et al. *Nucl. Phys. A* 424:605 (1984).
29. Gustafsson HÅ, et al. *Z. Phys.* A 321:389 (1985).
30. Beavis D, et al. *Phys. Rev. C* 33:1113 (1986).
31. Doss KGR, et al. *Phys. Rev. Lett.* 57:302 (1986).
32. Csernai LP, et al. *Phys. Rev. C* 34:1270 (1986).
33. Bock R, et al. *Modern Phys. Lett. A* 2:721 (1987).
34. Beckmann P, et al. *Modern Phys. Lett. A* 2:163 (1987).
35. Beckmann P, et al. *Modern Phys. Lett. A* 2:169 (1987).
36. Doss KGR, et al. *Phys. Rev. Lett.* 59:2720 (1987).
37. Bock R, Gutbrod HH, Siemiarczuk T. *Modern Phys. Lett. A* 3:237 (1988).
38. Gustafsson HÅ, et al. *Modern Phys. Lett. A* 3:1323 (1988).
39. Keane D, et al. *Phys. Rev. C* 37:1447 (1988).
40. Sengupta K, Singh G, Jain PL. *Europhysics Lett.* 5:135 (1988).
41. Demoulins M, et al. *Phys. Lett. B* 241:476 (1990).
42. Gosset J, et al. *Phys. Lett. B* 247:233 (1990).
43. Wang S, et al. *Phys. Rev. C* 44:1091 (1991).
44. Beavis D, et al. *Phys. Rev. C* 45:299 (1992).
45. Herrmann N. *Nucl. Phys. A* 553:739c (1993).
46. Donà R. PhD Thesis, University Padova (1994).
47. Elaasar M, et al. *Phys. Rev. C* 49:R10 (1994).
48. Wienold T. *GSI-Preprint GSI*-94-74 (1994).
49. Kugler A, et al. *Phys. Lett. B* 335:319 (1994).
50. Lambrecht D, et al. *Z. Phys. A* 350:115 (1994).
51. Ramillien V, et al (FOPI Collaboration). *Nucl. Phys. A* 587:802 (1995).
52. Partlan MD, et al (EOS Collaboration). *Phys. Rev. Lett.* 75:2100 (1995).
53. Wang S, et al (EOS Collaboration). *Phys. Rev. Lett.* 74:2646 (1995).
54. Zhang WM, et al. *Phys. Rev. C* 52:2643 (1995).
55. Chance J, et al (EOS Collaboration). *Phys. Rev. Lett.* 78:2535 (1997).
56. Crochet P. PhD Thesis, University Strasbourg (1996); Crochet P, et al (FOPI Collaboration).
57. Alard JP, et al (FOPI Collaboration). *Phys. Rev. Lett.* 69:889 (1992).
58. Wienold T. PhD Thesis, University Heidelberg (1993); GSI-Report GSI-93-28 (1993).
59. Doss KGR, et al. *Phys. Rev. C* 32:116 (1985).
60. Reisdorf W, et al (FOPI Collaboration). *Nucl. Phys. A* 612:493 (1997).
61. Huang MJ, et al. *Phys. Rev. Lett.* 77:3739 (1996).
62. Gutbrod HH, Poskanzer AM, Ritter HG. *Rep. Prog. Phys.* 52:1267 (1989).
63. Schmidt W, et al. *Phys. Rev. C* 47:2782 (1993).
64. Csernai LP, et al. *Phys. Rev. C* 28:2001 (1983).
65. Koch V, et al. *Phys. Lett. B* 241:174 (1990).
66. Bonasera A, Csernai LP. *Phys. Rev. Lett.* 59:630 (1987).
67. Bonasera A, Csernai LP, Schürmann B. *Nucl. Phys. A* 476:159 (1988).
68. Danielewicz P. *Phys. Lett. B* 146:168 (1984).
69. Yariv Y, Fraenkel Z. *Phys. Rev. C* 20:2227 (1979).
70. Cugnon J. *Phys. Rev. C* 22:1885 (1980).
71. Kitazoe Y, et al. *Phys. Rev. Lett.* 53:2000 (1984).
72. Pang Y, Schlagel TJ, Kahana SH. *Phys. Rev. Lett.* 68:2743 (1992).
73. Bertsch GF, DasGupta S. *Phys. Rep.* 160:189 (1988).
74. Cassing W, Mosel U. *Prog. Part. Nucl. Phys.* 25:235 (1990).
75. Blättel B, Koch V, Mosel U. *Rep. Prog. Phys.* 56:1 (1993).
76. Aichelin J, Stöcker H. *Phys. Lett. B* 176:14 (1986); Aichelin J. *Phys. Rep.* 202:233 (1991).
77. Molitoris JJ, et al. *Phys. Rev. C* 33:867 (1986).
78. Kahana D, et al. *Phys. Rev. Lett.* 74:4404 (1995).

79. Kortemeyer G, Daffin F, Bauer W. *Phys. Lett. B* 374:25 (1996).
80. Stock R, et al. *Phys. Rev. Lett.* 49:1236 (1982).
81. Harris JW, et al. *Phys. Rev. Lett.* 58:463 (1987).
82. Kruse H, Jacak BV, Stöcker H. *Phys. Rev. Lett.* 54:289 (1985).
83. Molitoris JJ, Stöcker H. *Phys. Rev. C* 32:346 (1985).
84. Friedman B, Pandharipande VR. *Nucl. Phys. A* 361:502 (1981).
85. Baron E, Cooperstein J, Kahana S. *Phys. Rev. Lett.* 55:126 (1985).
86. Gale C, Bertsch G, DasGupta S. *Phys. Rev. C* 35:1666 (1987).
87. Aichelin J, et al. *Phys. Rev. Lett.* 58:1926 (1987).
88. Welke GM, et al. *Phys. Rev. C* 38:2101 (1988).
89. Haddad F, et al. *Phys. Rev. C* 52:2013 (1995).
90. Blättel B, et al. *Phys. Rev. C* 43:2728 (1991).
91. Pan Q, Danielewicz P. *Phys. Rev. Lett.* 70:2062 (1993); 70:3523 (1993).
92. Zhang J, Das Gupta S, Gale C. *Phys. Rev. C* 50:1617 (1994).
93. Pak R, et al. *Phys. Rev. C* 54:2457 (1996).
94. Li Q, Wu JQ, Ko CM. *Phys. Rev. C* 39:849 (1989).
95. Serot BD, Walecka JD. *Adv. Nucl. Phys.* 16:1 (1986).
96. Maruyama T, et al. *Nucl. Phys. A* 573:653 (1994).
97. Fuchs C, et al. *J. Phys. G* 22:131 (1996).
98. Fuchs C, et al. *Nucl. Phys. A* 603:471 (1996).
99. Fuchs C, et al. *Phys. Lett. B* 381:23 (1996).
100. Hartnack C, et al. Report SUBATECH 96-13, Nantes, France (1996).
101. Klakov D, Welke G, Bauer W. *Phys. Rev. C* 48:1982 (1993).
102. Koch V, et al. *Nucl. Phys. A* 532:715 (1991).
103. Bass SA, et al. *Phys. Rev. C* 51:3343 (1995).
104. Li BA. *Nucl. Phys.* A570:797 (1994).
105. Gosset J, et al. *Phys. Rev. Lett.* 62:1251 (1989).
106. Pinkenburg CH, Hildenbrand K. *Acta Phys. Polonica* 27:243 (1996).
107. Kintner JC, et al (EOS Collaboration). *Phys. Rev. Lett.* 78:4165 (1997).
108. Li BA, Bauer W, Bertsch GF. *Phys. Rev. C* 44:2095 (1991).
109. Li BA, Bauer W. *Phys. Rev. C* 44:450 (1991).
110. Bass SA, et al. *Phys. Rev. Lett.* 71:1144 (1993).
111. Li GQ, Ko CM, Li BA. *Phys. Rev. Lett.* 74:235 (1995).
112. Li GQ, Ko CM, Brown GE. *Phys. Lett. B* 381:17 (1996).
113. Li GQ, Ko CM. *Phys. Rev. C* 54:1897 (1996).
114. Ritman JL, et al (FOPI Collaboration). *Z. Phys. A* 352:355 (1995).
115. Justice M, et al (EOS Collaboration). *Nucl. Phys.* A590:549c (1995).
116. Lee CH. *Phys. Rep.* 275:255 (1996).
117. Lee CH, et al. *Nucl. Phys. A* 585:401 (1995).
118. David C, et al. *Nucl. Phys. A* (1997). In press.
119. Ogilvie CA, et al. *Phys. Rev. C* 42:R10 (1990).
120. Krofcheck D, et al. *Phys. Rev. Lett.* 63:2028 (1989).
121. Ogilvie CA, et al. *Phys. Rev. C* 40:654 (1989).
122. Sullivan JP, et al. *Phys. Lett. B* 249:8 (1990).
123. Zhang WM, et al. *Phys. Rev. C* 42:R491 (1990).
124. Krofcheck D, et al. *Phys. Rev. C* 43:350 (1991).
125. Peter J. *Nucl. Phys. A* 545:173c (1992).
126. Shen WQ, et al. *Nucl. Phys. A* 551:333 (1993).
127. Lauret J, et al. *Phys. Lett. B* 339:22 (1994).
128. Buta A, et al. *Nucl. Phys. A* 584:397 (1995).
129. Zhi Yong He, et al. *Nucl. Phys. A* 598:248 (1996).
130. Pak R, et al. *Phys. Rev. C* 53:R1469 (1996).
131. Tsang MB, et al. *Phys. Rev. Lett.* 57:559 (1986).
132. Trautmann W, et al. *Phys. Rev. Lett.* 53:1630 (1984).
133. Westfall GD, et al. *Phys. Rev. Lett.* 71:1986 (1993).
134. Bertsch GF, Lynch WG, Tsang MB. *Phys. Lett. B* 189:384 (1987).
135. Xu HM. *Phys. Rev. Lett.* 67:2769 (1991).
136. Xu HM. *Phys. Rev. C* 46:R389 (1992).
137. de la Mota V, et al. *Phys. Rev. C* 46:677 (1992).
138. Krofcheck D, et al. *Phys. Rev. C* 46:1416 (1992).
139. Ma YG, et al. *Phys. Rev. C* 48:R1492 (1993).
140. Xu HM. *Phys. Rev. C* 47:891 (1993).
141. Tripathi RK, Townsend LW, Khan F. *Phys. Rev. C* 47:R935 (1993).
142. Zhou H, Li Z, Zhuo Y. *Phys. Lett. B* 318:19 (1993).
143. Li BA. *Phys. Rev. C* 48:2415 (1993).

144. Zhou H, Li Z, Zhuo Y. *Phys. Rev. C* 50:R2664 (1995).
145. Ma YG, Shen WQ. *Phys. Rev. C* 51:3256 (1995).
146. Soff S, et al. *Phys. Rev. C* 51:3320 (1995).
147. Lehmann E, et al. *Z. Phys. A* 355:55 (1996).
148. Lisa MA, et al (EOS Collaboration). *Phys. Rev. Lett.* 75:2662 (1995).
149. Gobbi A, et al (FOPI Collaboration). *Nucl. Phys. A* 583:499c (1995).
150. Li BA, Ko CM, Li GQ. *Phys. Rev. C* 54:844 (1996).
151. Pak R, et al. *Phys. Rev. Lett.* 78:1022 (1997); 78:1026 (1997).
152. Stöcker H, et al. *Phys. Rev. C* 25:1873 (1982).
153. Kapusta J, Strottman D. *Phys. Lett. B* 106:33 (1981).
154. Gutbrod HH, et al. *Phys. Lett. B* 216:267 (1989).
155. Popescu R, et al. *Phys. Lett. B* 331:285 (1994).
156. Leifels Y, et al. *Phys. Rev. Lett.* 71:963 (1993).
157. Tsang MB, et al. *Phys. Rev. C* 53:1959 (1996).
158. Brill D, et al (KAOS Collaboration). *Z. Phys. A* 355:61 (1996).
159. Brill D, et al (KAOS Collaboration). *Phys. Rev. Lett.* 71:336 (1993).
160. Jeong SC, et al (FOPI Collaboration). *Phys. Rev. Lett.* 72:3468 (1994).
161. Wang S, et al (EOS Collaboration). *Phys. Rev. Lett.* 76:3911 (1996).
162. Siemens PJ, Rasmussen JO. *Phys. Rev. Lett.* 42:880 (1979).
163. Bass SA, et al. *Phys. Rev. C* 51:R12 (1995).
164. Venema LB, et al. *Phys. Rev. Lett.* 71:835 (1993).
165. Hartnack C, et al. *Nucl. Phys. A* 538:53c (1992).
166. Hartnack C, et al. *Modern Phys. Lett. A* 13:1151 (1994).
167. Peilert G, et al. *Phys. Rev. C* 39:1402 (1989).
168. Danielewicz P. *Phys. Rev. C* 51:716 (1995).
169. Roy C, et al (FOPI Collaboration). *Z. Phys. A* 358:73 (1997).
170. Brill D, et al (KAOS Collaboration). *Z. Phys. A* 357:207 (1997).
171. Schubert A, et al (TAPS Collaboration). *Nucl. Phys. A* 583:385 (1995).
172. Novotny R, et al (TAPS Collaboration). *IEEE Trans. Nucl. Sci.* 38:379 (1991).
173. Senger P, et al (KAOS Collaboration). *Nucl. Inst. Meth. A* 327:393 (1993).
174. Li BA. *Phys. Lett. B* 319:412 (1993).
175. Pelte D, et al (FOPI Collaboration). *Z. Physik A* 357:215 (1997).
176. Nagamiya S, et al. *Phys. Rev. C* 24:971 (1981).
177. Hsi WC, et al. *Phys. Rev. Lett.* 73:3367 (1994).
178. Poggi G, et al (FOPI Collaboration). *Nucl. Phys. A* 586:755 (1993).
179. Petrovici M, et al (FOPI Collaboration). *Phys. Rev. Lett.* 74:5001 (1995).
180. D'Agostino M, et al. *Phys. Lett. B* 371:175 (1996).
181. Wieman H, et al (EOS Collaboration). *Nucl. Phys. A* 525:617c (1991); Rai G, et al IEEE Trans. Nucl. Sci. 37:56 (1990).
182. Marie N, et al. *Phys. Lett. B* 391:15 (1997).
183. Steckmeyer JC, et al. *Phys. Rev. Lett.* 76:4895 (1996).
184. Jeong SC, et al. *Nucl. Phys. A* 604:208 (1996).
185. Warren PG, et al (EOS Collaboration). Preprint Nucl-exp. 9610008.
186. Albergo S, et al. *Nuovo Cimento* 89A:1 (1985).
187. Pak R, et al. *Phys. Rev. C* 54:1681 (1996).
188. Barz HW, et al. *Nucl. Phys. A* 531:453 (1991).
189. Bauer W, et al. *Phys. Rev. C* 47:R1838 (1993).
190. Schussler F, et al. *Nucl. Phys. A* 584:704 (1995).
191. Heuer D, et al. *Phys. Rev. C* 50:1943 (1994).
192. Borderie IG, et al. Int. Symp. Large-Scale *Collect. Motion At. Nuclei*, Brolo, Italy (1996).
193. Bondorf JP, et al. *Phys. Rep.* 257:133 (1995).
194. Westfall GD, et al. *Phys. Rev. Lett.* 37: 1202 (1976).
195. Gosset J, Kapusta JI, Westfall GD. *Phys. Rev. C* 18:844 (1978).
196. Csernai LP, Barz HW. *Z. Phys. A* 296:173 (1980).
197. Hahn D, Stöcker H. *Phys. Rev. C* 37:1048 (1988).
198. Randrup J. *Comput. Phys. Commun.* 77: 153 (1993).
199. Kunde GJ, et al. *Phys. Rev. Lett.* 74:38 (1995).
200. Harris JW, et al. *Phys. Lett. B* 153:377 (1985).
201. Bondorf JP, Garpman SIA, Zimanyi J. *Nucl. Phys. A* 296:320 (1978).
202. Stöcker H, Gyulassy M, Boguta J. *Phys. Lett. B* 103:269 (1981).
203. Daffin F, Haglin K, Bauer W. *Phys. Rev. C* 54:1375 (1996).
204. Khoa Dao T, et al. *Nucl. Phys. A* 542:671 (1992).

205. Khoa Dao T, et al. *Nucl. Phys. A* 548:102 (1992).
206. Berenguer M, et al. *J. Phys. G: Nucl. Part. Phys.* 18:655 (1992).
207. Lang A, et al. *Z. Phys. A* 340:287 (1991).
208. ter Haar B, Malfliet R. *Phys. Rep.* 149:207 (1987).
209. Ono A, et al. *Prog. Theor. Phys.* 87:1185 (1992).
210. Feldmeier H. *Nucl. Phys. A* 514:322 (1990).
211. Angert A, et al. *Proc. Quark Matter Form. Heavy-Ion Collis.*, p. 557. Bielefeld, Germany: World Sci. (1982).
212. Barrette J, et al (E814 Collaboration). *Phys. Rev. Lett.* 70:2996 (1993).
213. Barrette J, et al (E877 Collaboration). *Phys. Rev. Lett.* 73:2532 (1994).
214. Gutbrod HH, et al. *Z. Phys.* A337:57 (1990).
215. Voloshin S, Zhang Y. *Z. Phys. C* 70:665 (1996).
216. Barrette J, et al (E877 Collaboration). *Phys. Rev. C* 51:3309 (1995).
217. Barrette J, et al (E877 Collaboration). *Phys. Rev. C* 55:1420 (1997).
218. Rai G, et al Proposal E895, LBL PUB-5399 (1993).
219. Awes TC, et al (WA80 Collaboration). *Phys. Lett. B* 381:29 (1996).
220. Wienold T, et al (NA49 Collaboration). *Nucl. Phys. A* 610:76c (1996).
221. Ollitrault JY. *Phys. Rev. D* 46:229 (1992); *Phys. Rev. D* 48:1132 (1993).
222. Mattiello R, et al. *Phys. Rev. Lett.* 74:2180 (1995).
223. Winckelmann LA, et al. *Nucl. Phys. A* 610:116c (1986).
224. Peilert G. *Nucl. Phys. A* 583:317 (1995).
225. Sorge H, et al. *Phys. Lett. B* 243:7 (1990).
226. Sorge H. *Phys. Lett. B* 373:16 (1996).
227. Sorge H. *Proc. HIPAGS 1996* Detroit, MI (1996).
228. Sorge H. *Z. Phys. C* 67:479 (1995).
229. Stöcker H, Maruhn JA, Greiner W. *Z. Phys. A* 290:297 (1979).
230. Bugaev KA, Gorenstein MI, Rischke DH. *Phys. Lett. B* 255:18 (1991).
231. Hung CM, Shuryak EV. *Phys. Rev. Lett.* 75:4003 (1995).
232. Rischke DH. *Nucl. Phys. A* 610:88c (1996).
233. Bjorken JD. *Phys. Rev. D* 27:140 (1983).
234. Jones PG, et al (NA49 Collaboration). *Nucl. Phys. A* 610:188c (1996).
235. Xu N, et al (NA44 Collaboration). *Nucl. Phys. A* 610:175c (1996).
236. Ahle L, et al (E866 Collaboration). *Nucl. Phys. A* 610:139c (1996).
237. Braun-Munzinger P, et al. *Phys. Lett. B* 344:43 (1995).
238. Lee KS, Heinz U, Schnedermann E. *Z. Phys. C* 48:525 (1990).
239. Schnedermann E, Sollfrank J, Heinz U. *Phys. Rev. C* 48:2462 (1993).
240. Bächler J, et al. *Phys. Rev. Lett.* 72:1419 (1994).
241. Braun-Munzinger P, et al. *Phys. Lett. B* 365:1 (1996).
242. Bearden IG, et al (NA44 Collaboration). *Phys. Rev. Lett.* 78:2080 (1997).
243. Abbott T, et al (E802 Collaboration). *Phys. Rev. C* 50:1024 (1994).
244. Leonidov A, Nardi M, Satz H. *Nucl. Phys. A* 610:124c (1996).
245. Chapman S, Nix JR. *Phys. Rev. C* 54:866 (1996).
246. Lisa MA. *Proc. Winter Workshop Nucl. Dyn., 11th*, Key West, FL (1995).
247. Bravina LV, et al. *Phys. Lett. B* 354:196 (1995).
248. Schnedermann E, Heinz U. *Phys. Rev. C* 50:1675 (1994).
249. Stachel J. *Nucl. Phys. A* 610:509c (1996).